Spatial modelling of local-scale biogenic and anthropogenic carbon dioxide emissions in Helsinki

JGR Atmospheres

RESEARCH ARTICLE
10.1029/2018JD029576

Spatial Modeling of Local-Scale Biogenic and Anthropogenic Carbon Dioxide Emissions in Helsinki

Leena Järvi[1,2], Minttu Havu[1], Helen C. Ward[3,4], Veronica Bellucco[5], Joseph P. McFadden[6], Tuuli Toivonen[2,7], Vuokko Heikinheimo[2,7], Pasi Kolari[1], Anu Riikonen[8], and C. Sue B. Grimmond[4]

[1]Institute for Atmospheric and Earth System Research/Physics, Faculty of Science, University of Helsinki, Helsinki, Finland, [2]Helsinki Institute of Sustainability Science, Faculty of Science, University of Helsinki, Helsinki, Finland, [3]Department of Atmospheric and Cryospheric Sciences, University of Innsbruck, Innsbruck, Austria, [4]Department of Meteorology, University of Reading, Reading, UK, [5]Department of Agriculture, University of Sassari, Sassari, Italy, [6]Department of Geography and Earth Research Institute, University of California, Santa Barbara, CA, USA, [7]Digital Geography Lab, Department of Geosciences and Geography, University of Helsinki, Helsinki, Finland, [8]Institute of Atmospheric and Earth System Research/Ecology, Faculty of Agriculture and Forestry, University of Helsinki, Helsinki, Finland

Abstract There is a growing need to simulate the effect of urban planning on both local climate and greenhouse gas emissions. Here, a new urban surface carbon dioxide (CO_2) flux module for the Surface Urban Energy and Water Balance Scheme is described and evaluated using eddy covariance observations at two sites in Helsinki in 2012. The spatial variability and magnitude of local-scale anthropogenic and biogenic CO_2 flux components at high spatial (250 m × 250 m) and temporal (hourly) resolution are examined by combining high-resolution (down to 2 m) airborne lidar-derived land use data and mobility data to account for people's movement. Urban effects are included in the biogenic components parameterized using urban eddy covariance and chamber observations. Surface Urban Energy and Water Balance Scheme reproduces the seasonal and diurnal variability of the CO_2 flux well. Annual totals deviate 3% from observations in the city center and 2% in a suburban location. In the latter, traffic is the dominant CO_2 source but summertime vegetation partly offsets traffic-related emissions. In the city center, emissions from traffic and human metabolism dominate and the vegetation effect is minor due to the low proportion of vegetation surface cover (22%). Within central Helsinki, human metabolism accounts for 39% of the net local-scale emissions and together with road traffic is to a large extent responsible for the spatial variability of the emissions. Annually, the biogenic emissions and sinks are in near balance and thus the effect of vegetation on the carbon balance is small in this high-latitude city.

Key Points:
- The high spatial variability of local-scale anthropogenic and biogenic CO_2 fluxes represented in central Helsinki
- The role of vegetation in the carbon balance is small in this high-latitude city
- The spatiotemporal variability of human metabolism has a large impact on local-scale spatial fluxes and net carbon emissions

Correspondence to:
L. Järvi,
leena.jarvi@helsinki.fi

Citation:
Järvi, L., Havu, M., Ward, H. C., Bellucco, V., McFadden, J. P., Toivonen, T., et al. (2019). Spatial modeling of local-scale biogenic and anthropogenic carbon dioxide emissions in Helsinki. *Journal of Geophysical Research: Atmospheres*, *124*, 8363–8384. https://doi.org/10.1029/2018JD029576

Received 29 AUG 2018
Accepted 17 MAY 2019
Accepted article online 4 JUN 2019
Published online 2 AUG 2019

Author Contributions

Conceptualization: Leena Järvi, Helen C. Ward, C. Sue B. Grimmond
Methodology: Leena Järvi, Minttu Havu, Helen C. Ward, Veronica Bellucco, Joseph P. McFadden, Tuuli Toivonen, Vuokko Heikinheimo, Pasi Kolari, Anu Riikonen, C. Sue B. Grimmond
Validation: Minttu Havu
Writing - Original Draft: Leena Järvi, C. Sue B. Grimmond
Investigation: Leena Järvi, Minttu Havu, C. Sue B. Grimmond
Resources: Anu Riikonen
Supervision: Leena Järvi
Visualization: Minttu Havu
Writing - review & editing: Minttu Havu, Helen C. Ward, Veronica Bellucco, Joseph P. McFadden, Tuuli Toivonen, C. Sue B. Grimmond

1. Introduction

The main driver for ongoing global warming is increased anthropogenic greenhouse gas emissions to the atmosphere. As anthropogenic activities concentrate in urban areas, these regions are estimated to be responsible for 30–40% of the world's anthropogenic greenhouse gas emissions (Marcotullio et al., 2013; Satterthwaite, 2008) of which carbon dioxide (CO_2) is the most important. This has stimulated cities to take actions to reduce their carbon emissions (Reckien et al., 2014; Rosenzweig et al., 2010) while seeking sustainable solutions to other challenges caused by urbanization and preparing adaptation and mitigation strategies for the changing climate. The challenges include, for example, biodiversity, thermal comfort, and flooding. To evaluate the benefits and disadvantages of different policies and practices on CO_2 emissions for existing conditions as well as under future climate and planning scenarios, integrated models simulating CO_2 surface exchange together with the other urban climate variables relevant for urban dwellers are needed. However, there are few urban ecosystem models that allow examination of these integrated effects with sufficient temporal and spatial resolution that planning choices can be compared. High resolution models are also key to quantifying large-scale emissions. Errors in the timing, location, and magnitude of urban emissions can cascade into the remaining flux components in carbon inversion studies where anthropogenic CO_2 emissions are used as boundary condition for other modeling components (Hutyra et al., 2014).

Urban land surface models provide an excellent base for integrated urban ecosystem models as they simulate the surface exchange of energy and commonly the components of the hydrological cycle at a local scale. Extending these models to local-scale CO_2 emissions allows the highly spatially and temporally variable anthropogenic CO_2 emissions to be considered. The net emissions are a complex function of emissions from road traffic, household activities, industry and other point sources, vegetation, and human metabolism. The same sources, excluding vegetation, are also responsible for anthropogenic heat emissions in urban areas (Allen et al., 2011) further supporting the integration of urban climate and CO_2 emission models. In recent years, spatial road traffic (Brondfield et al., 2012; Gately et al., 2017; Lee et al., 2017) and fossil fuel carbon emissions (Gurney et al., 2012, 2017) in cities have been examined and local hot spots identified, but the methodologies have not had any links to the heat emissions. Urban land surface models need to account for both the anthropogenic and biogenic components that modify the net ecosystem exchange (NEE) of CO_2. The latter includes both emissions by vegetation and soil respiration as well as carbon uptake via photosynthesis. The impact of vegetation on NEE in urban areas has been quantified by urban eddy covariance (EC) flux studies (Crawford et al., 2011; Järvi et al., 2012; Menzer et al., 2015; Nordbo et al., 2012a; Ward et al., 2015). However, these have limited spatial extent relative to the city scale. At the city scale, street trees sequester only a minor proportion (0.08–3.4%) of urban transportation (Russo et al., 2015) and net (Escobedo et al., 2010; Tang et al., 2016) CO_2 emissions. These biomass-based studies focus only on urban street trees, whereas studies accounting for urban vegetation and biomass more widely have quantified higher proportions. In Florence, Italy, green areas sequester 6.2% of the total direct anthropogenic CO_2 emissions (Vaccari et al., 2013) and in Massachusetts, USA, a ratio of biogenic sink strength to fossil fuel emissions of 14% was found (Hardiman et al., 2017). Often, process models developed for natural ecosystems are used to estimate biogenic carbon budgets within urban areas ignoring the urban effects. Hardiman et al. (2017) corrected the biogenic components for urban effects but used model parameterizations developed for natural vegetation. Also, the relatively coarse spatial (10^2–10^3 m) and temporal resolutions of nonurban models are not ideal for studies examining the effect of urban planning alternatives on cities' carbon balances. The role of vegetation in sequestering CO_2 emitted from anthropogenic activities may play an important role in the surface-atmosphere exchange of CO_2 and furthermore on a city's carbon balance (Sargent et al., 2018). This CO_2 assimilation is one of the many ecosystem services that urban vegetation can deliver (Niemelä et al., 2010).

Here both local-scale anthropogenic and biogenic surface-atmosphere exchanges of CO_2 are incorporated into the urban land surface model SUEWS (Surface Urban Energy and Water balance Scheme, Järvi et al. (2011)). The model is evaluated against EC observations at two contrasting sites differing in surface cover and human activities in Helsinki. Using the model, the spatial and temporal variability of both anthropogenic and biogenic components of the net surface exchange are quantified across Helsinki.

2. Model Description

Urban surface-atmosphere exchange of CO_2 is included within the SUEWS version V2018b (Ward et al., 2016). This already has the capability of simulating the urban energy and water cycles at a local scale or neighborhood scale using commonly measured meteorological variables and surface information including surface cover fractions (buildings, paved surfaces, evergreen trees/shrubs, deciduous trees/shrubs, grass, bare soil, and water), population densities, and tree and building heights. In SUEWS, the surface is divided into seven parallel surface types, and the rates of evaporation-interception are calculated for each. Below each surface type there is a single soil layer. Latent heat flux at each time step (default 5 min) is calculated with a modified Penman-Monteith equation (Grimmond & Oke, 1991) and sensible heat flux as a residual from the energy balance equation. The model has submodels for net all-wave radiation, storage and anthropogenic heat fluxes, snow, and irrigation (Järvi et al., 2011, 2014; Offerle et al., 2003). The advantage of SUEWS when compared to other urban land surface schemes is that it contains a parameterization for downward long-wave radiation (Loridan et al., 2010), and it does not have separate tiles for urban and vegetation surface fractions, but rather a dynamic interaction between the surface types is allowed. SUEWS has demonstrated good performance against hydrological observations, and EC-measured turbulent sensible and latent heat fluxes in several cities in Europe, North America, and Asia (e.g., Alexander et al., 2016; Ao et al., 2018; Järvi et al., 2011, 2017; Kokkonen et al., 2018, 2019; Ward et al., 2016).

The new module in SUEWS presented here determines the local-scale surface exchanges of CO_2 (F_c, $\mu mol \cdot m^{-2} \cdot s^{-1}$) allowing the impact of urban planning choices and climate scenarios on the cycles of energy,

water, and CO_2 to be studied in detail. The CO_2 exchange module accounts for both the anthropogenic ($F_{c,ant}$) and biogenic components ($F_{c,bio}$)

$$F_c = F_{c,ant} + F_{c,bio} = (F_M + F_V + F_B + F_P) + (F_{pho} + F_{res}), \quad (1)$$

where F_M are CO_2 emissions from human metabolism, F_V emissions from traffic, F_B emissions from building energy and heating/cooling combustion (with natural gas, coal, and wood), F_P emissions from local-scale point sources, F_{pho} is photosynthesis, and F_{res} is respiration. In the current model version, CO_2 absorption and release by water surfaces are not accounted for and are assumed to be zero. Positive values indicate sources of CO_2 and negative values sinks with respect to the atmosphere.

SUEWS simulates the carbon emissions at the local scale neighbourhoods where many of the urban planning interventions, such as requiring building of new green areas or restricting vehicular traffic, occur. This scale of simulation provides the lower boundary conditions for the planetary boundary layer but allows for spatial variability across the urban area. Many studies focus on carbon balance of the whole city (Bréon et al., 2015; Sargent et al., 2018) with it treated as a volume with lateral boundaries to the upper limit of the boundary layer. Using the local scale, we can capture differences in neighborhood behaviors so that important temporal, for example diurnal and daily (e.g., weekday/weekend), variations become apparent. The vertical scale extends from the constant flux layer to the subsurface to cover the relevant time scale. Thus, very tall stacks emitting CO_2 are not captured unless SUEWS is coupled to a three-dimensional atmospheric model to determine when that air is entrained back into the boundary layer. Most notably, work and home locations, parks and roads, and so forth, are evident. Thus, the feedback between surface processes and the overlying air volume are accounted for and the impact of planning of governance interventions at the short term (e.g., permitted behaviors such as changing work hour) or longer term (e.g., street tree planting and urban design) can be captured. Different impacts across a city or implementation of different carbon reduction strategies can also be evaluated.

2.1. Anthropogenic Components

The local-scale anthropogenic carbon emissions are estimated using a similar inventory approach as used to estimate anthropogenic heat emissions from urban areas (Allen et al., 2011; Grimmond, 1992; Sailor & Lu, 2004; Ward et al., 2015). The CO_2 emissions simulated within the model are separated into human metabolism, traffic emissions and building energy, and heating/cooling combustion. Other local-scale sources can be user-defined with their emission strengths. Traditionally, the anthropogenic heat flux (Q_F) in SUEWS is calculated with a simple model based on heating and cooling degree days, but now a modified inventory approach is also included. Hourly heat ($Q_{M,h,d}$, $W \cdot m^{-2}$) and carbon ($F_{M,h,d}$, $\mu mol \cdot m^{-2} \cdot s^{-1}$) emissions from human metabolism are calculated using

$$Q_{M,h,d} = p_{h,d} \cdot H_{a,h,d} \cdot E_M \quad (2)$$

and

$$F_{M,h,d} = p_{h,d} \cdot H_{a,h,d} \cdot C_M, \quad (3)$$

where $p_{h,d}$ is the population density by day (d in our case workdays [wd] or weekends [we]) and by hour (hr, cap/ha), $H_{a,h,d}$ activity by hour calculated from the diurnal profiles for population $H_{P,d}$ and activity $H_{A,d}$, and E_M and C_M metabolic energy and CO_2 release per person ($W \cdot cap^{-1}$ and $\mu mol \cdot CO_2 \cdot s^{-1} \cdot cap^{-1}$). E_M and C_M vary between nighttime minimum and maximum values ($E_{M(min,max)}$ and $C_{M(min,max)}$) based on the activity profile $H_{a,h,d}$.

Hourly traffic related heat ($Q_{V,h,d}$) and carbon emissions ($F_{V,h,d}$) on different days are calculated from

$$Q_{V,h,d} = Tr_d \cdot E_{h,d} \cdot H_{T,d} \quad (4)$$

$$F_{V,h,d} = Tr_d \cdot E_{c,d} \cdot H_{T,d}, \quad (5)$$

where Tr_d is the mean daily traffic rate within the study area ($veh \cdot day^{-1} \cdot area^{-1}$), $H_{T,d}$ the diurnal traffic profiles, and $E_{h,d}$ and $E_{c,d}$ traffic emission factors for heat ($J \cdot km^{-1} \cdot veh^{-1}$), and CO_2 ($kg \cdot km^{-1} \cdot veh^{-1}$) on weekdays and weekends. User-supplied emission factors can vary across the modeling domain if available. This allows different vehicle distributions and speeds in different areas to be considered.

The required mean traffic and population values are relatively easily obtained in many areas. For building related local-scale heat and carbon emission, inventory information can be more difficult to obtain. In SUEWS daily values are estimated from the cooling (CDD) and heating degree days (HDD)-based model of Q_F (Järvi et al., 2011)

$$Q_{F,d} = p_{h,d}[a_{0,d} + a_{1,d}\mathrm{CDD} + a_{2,d}\mathrm{HDD}], \tag{6}$$

where $a_{0,d}$ is the nontemperature-related base value of Q_F including heat emissions from traffic, human metabolism and electricity usage, and $a_{1,d}$ and $a_{2,d}$ are temperature-related coefficients above and below a base human comfort temperature (18.2 °C; Sailor & Vasireddy, 2006). For convenience, the different components in equation (6) are expressed as

$$Q_{F,d} = Q_{F,\mathrm{base}} + Q_{F,\mathrm{cool}} + Q_{F,\mathrm{heat}}. \tag{7}$$

The hourly building-related heat emissions ($Q_{B,h,d}$) are

$$Q_{B,h,d} = (Q_{F,\mathrm{base}} \cdot fr_{\mathrm{QF,base,BEU},d}) + Q_{F,\mathrm{heat}} + Q_{F,\mathrm{cool}}, \tag{8}$$

where $fr_{\mathrm{QF,base,BEU},d}$ is the fraction of the nontemperature-related base value coming from building energy use on workdays/weekends.

Depending on the city, the building heating and energy production can take place at either the domestic or the district level. In the first, biomass, gas, wood, or coal can be burned for energy and heating within the study area creating local CO_2 emissions, whereas in the latter no local CO_2 emissions from buildings take necessarily place. In SUEWS, the possibility for both options is enabled by introducing the fraction of fossil fuels used for heating (fr_{heat}) and energy (fr_{nonheat}) within the study area

$$F_{B,h,d} = [fr_{\mathrm{heat}}(Q_{F,\mathrm{heat}} + Q_{F,\mathrm{cool}}) + fr_{\mathrm{nonheat}} \cdot Q_{F,\mathrm{base}} \cdot fr_{\mathrm{QF,base,BEU},d}] \cdot E_{\mathrm{CO2perJ}}. \tag{9}$$

E_{CO2perJ} is the emission factor for fuels used in building energy use. Emissions from single-point sources such as power plants and industrial activities can be included as model inputs, but in many cases, these are located outside the model domain or at heights that are beyond the local scale of interest.

2.2. Biogenic Components

Commonly in ecological models, the carbon uptake (F_{pho}) is estimated based on light response curves (Lasslop et al., 2010). In SUEWS, the possibility to calculate photosynthesis both with rectangular and nonrectangular hyberbola equations (Bellucco et al., 2017; Ruimy et al., 1995) is included. These methods, however, do not consider the effect of the local conditions on F_{pho}, and thus, it can also be calculated using an empirical canopy-level photosynthesis model, where the potential photosynthesis ($F_{\mathrm{pho,max},i}$) is modified for different environmental factors (Mäkelä et al., 2008)

$$F_{\mathrm{pho}} = \sum_i (f_i F_{\mathrm{pho,max},i} \mathrm{LAI}_i) f(T_{\mathrm{air}}) f(\Delta q) f(\Delta\theta) f(K_\downarrow), \tag{10}$$

where the sum is the product of potential photosynthesis and leaf area index (LAI_i) over the three vegetated surfaces i weighted with their surface fraction f_i and $f(T_{\mathrm{air}})$, $f(\Delta q)$, $f(\Delta\theta)$, and $f(K_\downarrow)$ are the responses of photosynthesis on air temperature (T_{air}), specific humidity (Δq), soil moisture deficit ($\Delta\theta$), and shortwave radiation ($K_\downarrow$). For reliable estimation of biogenic components f_i should include also overhanging vegetation on impervious surfaces such as street trees and shrubs. With the parameters derived from urban observations the local urban climate is accounted for (Appendix A). T_{air} and Δq from the model input or local values at 2-m height calculated within the model (Sun & Grimmond, 2019) can be used with the latter allowing for spatial variability of F_{pho}. $\Delta\theta$ is spatially variable with simulated response from both the energy and water flux exchanges within SUEWS.

Soil and vegetation respiration F_{res} ($\mu\mathrm{mol}\cdot\mathrm{m}^{-2}\cdot\mathrm{s}^{-1}$) is assumed to follow the exponential dependency on air temperature

$$F_{\mathrm{res}} = \sum_i f_i \max(a_i \cdot \exp(T_{\mathrm{air}} b_i), 0.6), \tag{11}$$

where a_i and b_i are user-selected empirical constants. Although, soil respiration depends on the soil temperature rather than air temperature, the latter is used to minimize model input. Sensitivity tests made by Bellucco et al. (2017) suggest that this leads to reasonable respiration estimates. However, winter soil may remain warmer than air resulting in carbon emissions via decomposition of organic matter in winter, even through snow (Pumpanen et al., 2015). Thus, we limit the soil respiration to 0.6 $\mu mol \cdot m^{-2} \cdot s^{-1}$ based on winter time soil chamber measurements made in a boreal forest in central Finland (see Appendix B). In Helsinki this minimum value is exceeded only on 0.09% of the hours analyzed.

3. Site and Data Description

3.1. Site Characteristics and Measurements

The CO_2 model is evaluated against direct EC measurements made at two sites with contrasting source area characteristics in Helsinki, Finland, in 2012. The semiurban Kumpula, located 4 km northeast of the city center, is classified as local climate zone (LCZ) 6 (Stewart & Oke, 2012). Half of the surroundings within 1 km of the 31-m measurement mast is vegetated (Karsisto et al., 2015). North of the tower (320–40°, hereafter Ku1) is the university campus area and further away suburban low height apartment buildings with small gardens. To the east (40–180°, Ku2) emissions come from one of the main roads leading to the Helsinki city center. The area between the road and mast (closest distance 150 m) is covered with broadleaf forest. To the southwest (180–320°, Ku3) lies parks, the University Botanical Garden, and allotment gardens. In this direction, the closest road is 800 m from the measurement mast. The second site, Hotel Torni, situated in the highly built-up city center at 60 m (LCZ = 2) (Karsisto et al., 2015; Nordbo et al., 2013) has within 1-km radius circle, a mean building height of 18 m, and vegetation cover fraction of 20% consisting of street trees and a few parks. Table 1 summarizes the mean site characteristics of both sites.

The wind components are measured with an ultrasonic anemometer (USA-1, Metek GmbH, Germany). The carbon dioxide mixing ratio is measured with a closed-path infrared gas analyzer (LI-7000, LI-COR, Lincoln, NE, USA) at Kumpula and with an enclosed-path infrared gas analyzer (LI-7200, LI-COR) at Torni. At both sites, 60-min flux values are calculated using commonly accepted procedures following Nordbo et al. (2012b). After quality flagging and stationarity test (limit of 60% used) 3.6% ($N = 318$) of F_c are missing from Kumpula in 2012. At the city center site, a building structure disturbs the measurements in the 40–150°direction which leads to greater removal of flux data ($N = 3,971$, 45.2% in 2012; Järvi et al., 2018). No filtering based on friction velocity, kurtosis and skewness is made. For calculation of observed annual NEE, the missing data are gap filled using median diurnal cycle method, where gaps are filled using the monthly median diurnal cycle values calculated separately for weekdays and weekends. This has been found to give good correspondence with respect to more comprehensive and complex gap filling method artificial neural network at the Kumpula site (Järvi et al., 2012). The uncertainty of the annual cumulative flux value at the city center due to the large amount of missing data is up to 12% as calculated from the simultaneous measurements of second EC system located on the opposite side of the building structure (Järvi et al., 2018).

The meteorological forcing data are mostly measured at Kumpula. These include T_{air} (Pt-100, "in-house"), wind speed (Thies Clima 2.1x, Gottingen, Germany), and $K_{\downarrow}$ (CNR1, Kipp&Zonen, Delft) measured on the EC mast 31 m above the ground level. In addition, air pressure (DPA500, Vaisala Oyj, Vantaa, Finland), relative humidity (HMP243, Vaisala Oyj), and precipitation (rain gauge, Pluvio2, Ott Messtechnik GmbH, Germany) are measured on the roof of a nearby building at 24 m. For model runs in city center, T_{air} (HMP45D, Vaisala Oyj) measured 550 m southeast of the EC Torni at 53 m is used.

3.2. Surface Data

Surface characteristics for Helsinki are obtained from a variety of sources. Surface cover fractions and the height of buildings and trees are from airborne lidar data with a resolution of 2 m (Nordbo et al., 2015). The vegetation is classified into trees, low vegetation and shrubs, and grass. Low vegetation is assumed to be all deciduous, whereas trees are 60% deciduous and 40% evergreen, based on assuming street trees are half and forest trees 25% deciduous as is the case in southern coastal region of Finland (Korhonen et al., 2015). Population densities from the SeutuCD database for 2011 (HSY, 2011) provide the nighttime population. Daytime population can increase significantly (50–100%; Sailor et al., 2015) particularly in city centers, and for realistic human carbon emissions these need to be accounted for. The mean daily information on spatial movement of people is obtained from the Monitoring System of Urban Structure (YKR), produced by the Finnish Environment Institute and Statistics Finland. In YKR, the nocturnal population is based on

Table 1
Site Characteristics Within a 1-km Radius Circles Around the EC Measurement Towers (Kumpula and Torni) in Helsinki

Variable	Kumpula			Torni
Latitude	60°12′10.14″ N			60°10′04.09″ N
Longitude	24°57′40.06″ E			24°56′19.28″ E
Time zone	02 UTC			02 UTC
z (m)	31			60
alt (m)	26			15
DLS	86–303			86–303
	Ku1	Ku2	Ku3	
LCZ	3	6	9	2
A (ha)	70	122	122	314
fr_{build}	0.20	0.15	0.11	0.37
fr_{paved}	0.42	0.39	0.30	0.40
fr_{evergtr}	0.08	0.07	0.10	0.00
fr_{decidtr}	0.14	0.13	0.17	0.10
fr_{grass}	0.16	0.25	0.32	0.07
fr_{water}	0.00	0.01	0.00	0.01
fr_{heat}	0.05	0.05	0.05	0.00
fr_{nonheat}	0	0	0	0
$fr_{\text{QF,base,BEU,wd}}$	0.57	0.43	0.80	0.70
$fr_{\text{QF,base,BEU,we}}$	0.67	0.51	0.82	0.71
z_{build} (m)	10.4	11.5	12.6	17.9
z_{tree} (m)	10.0	8.8	8.5	8.3
$p_{\text{night,d}}$(inh·ha^{-1})	30.7	37.5	43.6	80.9
$p_{\text{day,wd}}$(inh·ha^{-1})	8.9	40.9	28.8	344.5
$p_{\text{day,we}}$ (inh·ha^{-1})	15.8	39.8	33.5	283.2
Tr_{wd} (veh km·m^{-2}·day^{-1})	0.0182	0.0637	0.0045	0.0920
Tr_{we} (veh km·m^{-2}·day^{-1})	0.0124	0.0434	0.0031	0.0706
$a_{0,wd}$ (W ha·cap^{-1}·m^{-2})	0.1337	0.1672	0.0958	0.1105
$a_{1,d}$ (W ha·cap^{-1}·m^{-2}·K^{-1})	0	0	0	0
$a_{2,\text{d}}$ (W ha·cap^{-1}·m^{-2}·K^{-1})	0.0149	0.0149	0.0149	0.0149
$a_{0,\text{we}}$ (W ha·cap^{-1}·m^{-2})	0.1153	0.1433	0.0937	0.1084

Note. EC = eddy covariance.

the Finnish population registry (same data used in the SeutuCD database) collected at the level of buildings and aggregated to the 250-m grid squares. The dynamic daytime population is calculated for working population based on work trip information. The movement is calculated as the difference of the nighttime population and the incoming and outgoing work journeys per grid square, as registered in YKR data. The YKR population data are for 2012 and the work journeys for 2010. The activity ($H_{A,d}$) and population ($H_{P,d}$) profiles determine the change between daytime and nighttime human-based CO_2 emissions (Figure 1).

Mean traffic rates are reported by street for Helsinki for workdays. Weekend traffic rates are 77% in city center and 68% at Kumpula of the workday values at city center and access road online traffic monitoring points (Kurppa et al., 2015). For simplicity, the same fractions are used to calculate the workday and weekend population densities (i.e., assuming fewer people move in and out of the city center during weekends than on workdays). Traffic counts are converted to vehicle kilometers per area per day by estimating the mean distance traveled within the area of interest. Traffic measurements provide traffic profiles ($H_{T,d}$) for converting daily traffic emissions to hourly values (Figure 1). $H_{P,d}$ follow those of traffic, whereas $H_{A,d}$ increase 1 hr

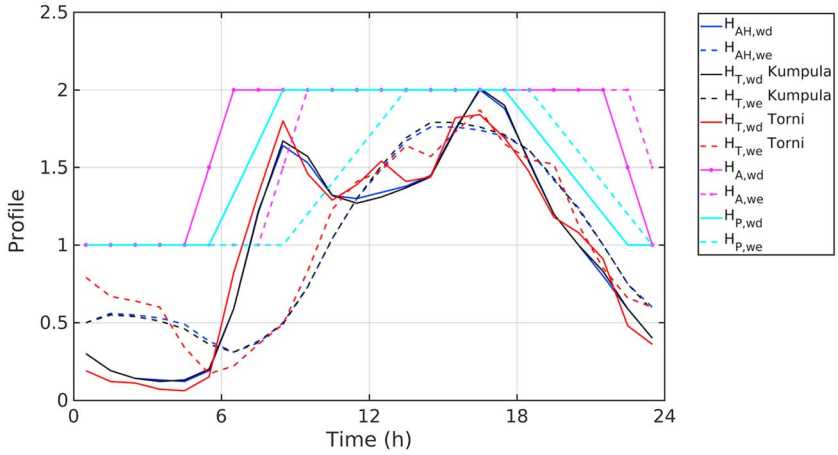

Figure 1. Weekday and weekend diurnal profiles of activity ($H_{A,d}$), traffic ($H_{T,d}$) and population ($H_{P,d}$). $H_{AH,d}$ are the emission profiles originally used in Surface Urban Energy and Water balance Scheme to describe anthropogenic heat emissions without partitioning to the different emissions sources. Traffic profiles are different for city center (Torni) and suburbs (Kumpula). $H_{P,d}$ is scaled using both nighttime and daytime populations. There can also be smaller daytime population density values.

before people start to move from their homes and 1 hr after people have returned to their homes. All profiles take into account the daylight saving time.

4. Model Runs

We conduct two types of model runs. First, SUEWS is run for the approximate source areas of the EC measurement sites in Helsinki in order to evaluate its performance and the contributions of different sources on the net CO_2 exchange. Second, the spatial variability of the emissions and the contributions of different components to the net CO_2 emissions in central Helsinki are assessed. To calculate the biogenic fluxes, the simulated 2-m air temperature and specific humidity are used to allow spatial variability of $F_{c,\mathrm{bio}}$. The parameters used to calculate F_{pho} and F_{res} have been derived from urban observations (Appendix A).

4.1. Model Evaluation in Helsinki

The model is evaluated using the EC-measured net CO_2 exchanges at two sites. Good model performance at the same sites has been found for sensible and latent heat fluxes (Karsisto et al., 2015). For both sites the EC flux source areas (Kurppa et al., 2015; Nordbo et al., 2013) extend approximately 1 km around the EC towers. As source area models have large uncertainties for urban areas, further refinement is not warranted for individual hours. The site heterogeneity around Kumpula is addressed by simulating the three 1-km radius sectors separately, whereas around Torni the source/sink distribution is relatively homogeneous and thus no separation to different sectors is made. The surface parameters for the model simulations are calculated for the 1-km radius sectors. The model outputs are then combined based on the prevailing measured wind direction for each hour. As EC observations (prior to the study year 2012) for Ku3 are used to derive parameter values for F_{pho} and F_{res}, the modeled values are not completely independent of the Ku3 observations. On the other hand, observations from Ku1, Ku2, and Torni have not been used in model development.

The hourly meteorological forcing data are used to undertake calculations with a 5-min time step. The data are averaged back to 60-min for subsequent analyses. SUEWS is run for two consecutive years, with the first year (2011) being a spin-up period and the actual model evaluation made for 2012. Tables 1 and 2 summarize the parameters used in the model runs. At both sites, nighttime populations are assumed to be the same on workdays and weekends and thus ignore some nocturnal activities keep captured in the daytime mobility. In Kumpula, daytime population densities decrease associated with people traveling to work from the area on workdays. Whereas in the city center, the population densities increase to 345 from 81 inh·ha^{-1}. On weekends people move less (32% and 23% in Torni and Kumpula, respectively) based on the traffic rates. In Helsinki energy and to a large extent building heating are provided via district energy networks. Wood burning mainly occurs in single-family houses, whereas in other areas this is expected to be negligible. In Kumpula, the fraction of CO_2 emissions from building heating (fr_{heat}) is estimated to be 5% and at Torni

Table 2
Nonsite-Dependent Model Parameters

Parameter	Value	Reference
$C_{M(\min)}$ (μmol $CO_2 \cdot s^{-1} \cdot cap^{-1}$)	120	Ward et al. (2013)
$C_{M(\max)}$ (μmol $CO_2 \cdot s^{-1} \cdot cap^{-1}$)	280	Moriwaki and Kanda (2004)
$E_{c,d}$ ($kg \cdot km^{-1}$)	0.285	Järvi et al. (2012)
$E_{h,d}$ ($kJ \cdot km^{-1}$)	$4.11 \cdot 10^6$	This study
$E_{CO2perJ}$ (μmol $CO_2 \cdot J^{-1}$)	0.0025	Tilastokeskus (2018)

Note. See Notation for details.

zero. The heat release per vehicle per meter of travel ($E_{h,d}$) in Table 2 has been calculated as a product of the net heat of combustion of gasoline ($46.5 \cdot 10^6$ $J \cdot kg^{-1}$), fuel density (0.75 $kg \cdot L^{-1}$) and mean fuel economy (8.5 $km \cdot L^{-1}$; Sailor & Lu, 2004).

Model evaluation is done by thermal seasons defined by the 5-day mean T_{air}: winter <0 °C (27 October to 28 February 2012), summer >10 °C (8 May to 22 September 2012) and between spring (1 March to 7 May 2012) and fall (23 September to 26 October 2012).

4.2. Spatial Model Runs

The spatial variability of net CO_2 exchange (resolution 250 m × 250 m) is studied for a 6 × 9 km^2 domain (Figure 2a). The parameters for each grid's surface and anthropogenic activities, based on a split between dense city center and suburban area (Figure 2a), follow Torni and Ku2 (Table 1). The only exceptions are fr_{heat} which is zero except for the single-family housing areas located northeast and northwest of the model domain, and a_{grass} and b_{grass} for which values used at Torni and obtained from soil chamber measurements are used in the whole domain (Table A1).

The access roads leading to Helsinki city center are evident on the traffic map (Figure 2b) with values reaching 68,500 $veh \cdot day^{-1}$. In the city center, typical daily traffic counts are 10,000–30,000 $veh \cdot day^{-1}$. The difference between daytime and nighttime population densities is striking (Figured 2c and 2d), with population hot spots varying. At night, the densest neighborhoods are in west-northwest and north (maximum 440 $inh \cdot ha^{-1}$) of the city center which has a few residents. During the day, people travel to the city center with maximum densities reaching 1,873 $inh \cdot ha^{-1}$. The number of people within the model domain increases from (nighttime) 179,000 to (daytime) 466,000, with people commuting from the rest of Helsinki and neighboring cities within the Helsinki metropolitan region. A secondary hot spot northwest of the city center (1,800 $inh \cdot ha^{-1}$) is associated with the University of Helsinki's medical campus and the main hospital.

4.3. Evaluation Statistics

The model performance is evaluated using common statistical metrics including a Pearson correlation coefficient (r), root-mean-square error (RMSE, $\mu mol \cdot m^{-2} \cdot s^{-1}$), normalized RMSE, mean absolute error (MAE, $\mu mol \cdot m^{-2} \cdot s^{-1}$) and normalized mean absolute error (nMAE). The normalized statistics have the form

$$\mathrm{nRMSE} = \frac{\mathrm{RMSE}}{\max(F_{c,\mathrm{obs}}) - \min(F_{c,\mathrm{mod}})} \tag{12}$$

and

$$\mathrm{nMAE} = \frac{\mathrm{MAE}}{\max(F_{c,\mathrm{obs}}) - \min(F_{c,\mathrm{mod}})}. \tag{13}$$

The difference in modeled and observed cumulative sums is expressed as a percentage change

$$\mathrm{D} = 100 \cdot \frac{F_{c,\,\mathrm{obs}} - F_{c,\,\mathrm{mod}}}{F_{c,\,\mathrm{obs}}}. \tag{14}$$

5. Results

5.1. Model Performance and Source Apportionment at the EC Sites in Helsinki

SUEWS simulates the diurnal behavior of all three Kumpula land use sectors (Ku1–Ku3; Figure 3 and Table 3) well with the largest MAE (1.46–1.69 $\mu mol \cdot m^{-2} \cdot s^{-1}$) in Ku1 in summer and fall. The model has particular difficulty in simulating nocturnal F_c in summer. In Ku2 and Ku3, MAE are between 0.10 and

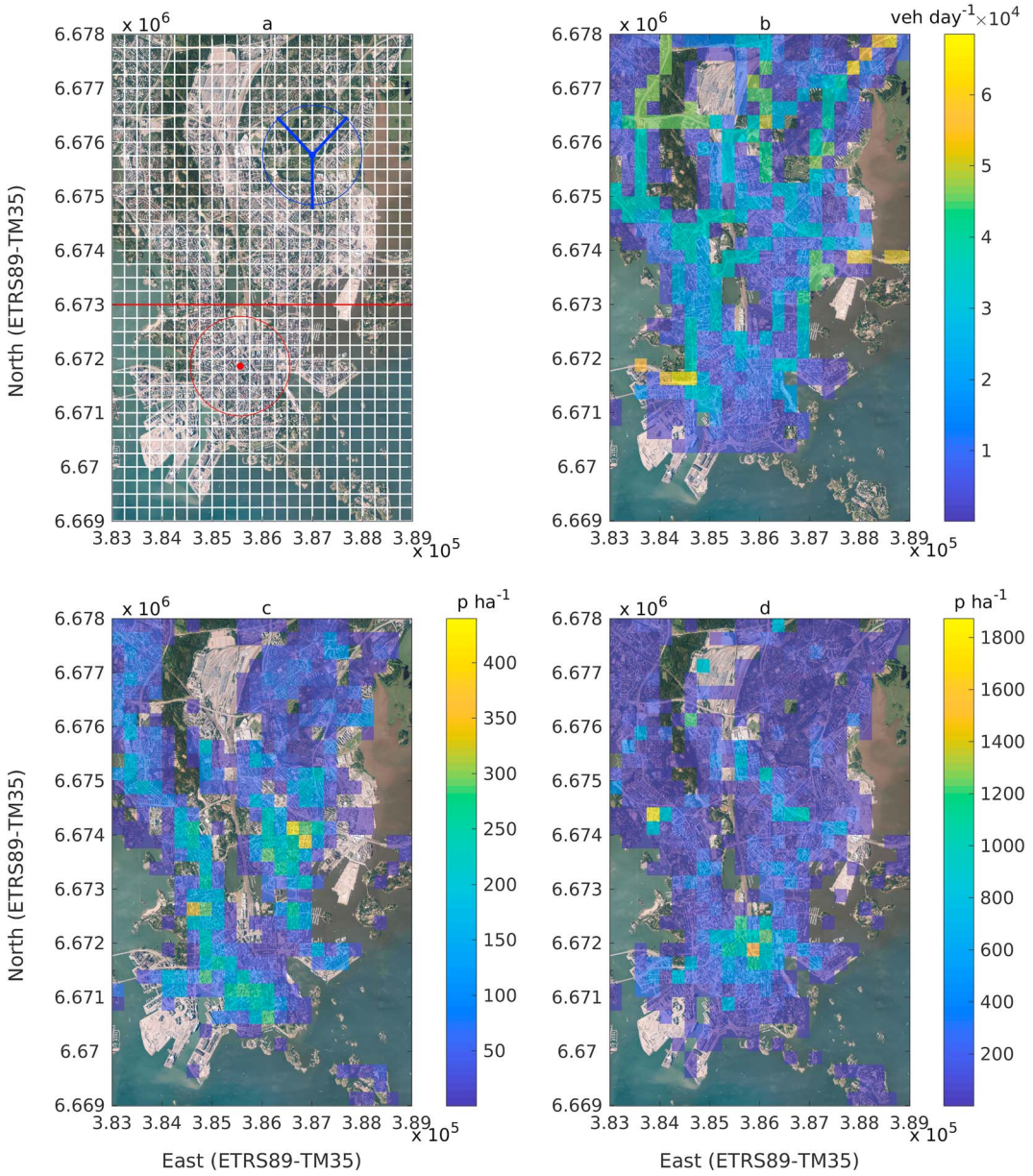

Figure 2. Study area 6 × 9 km^2 (Kaupunkimittausosasto, Helsinki, 2017) (a) with 250-m × 250-m grids and location of the eddy covariance sites Kumpula (blue) and Torni (red). City center and suburban areas (separated by red line) use different model parameters (Table 1). (b) Mean workday daily traffic rates. (c) Nocturnal population densities. (d) Daytime population densities. Note different scales between daytime and nighttime population density maps. See section 3.2 for data sources.

1.28 μmol·m^{-2}·s^{-1}. The same pattern is seen in nMAE with values 0.02–0.05 (winter–fall) in Ku1, 0.00–0.02 (summer–spring) in Ku2, and 0.00–0.02 (summer–spring) in Ku3. For Ku1, some observations are within the roughness sublayer because of the nearby tall buildings and therefore may not be necessarily representative of the local CO_2 surface exchange (i.e., greater uncertainty). Also, in our simulations the only component contributing to the building emissions is heating degree days-driven emissions and thus the simulations do not account for possible recreational household emissions in summer, for example, from heating of saunas. Based on RMSE and nRMSE, the model has the most challenge for Ku2, with the values ranging between 2.10–3.00 μmol·m^{-2}·s^{-1} (winter–summer) and 0.03–0.07 μmol·m^{-2}·s^{-1} (winter–fall), whereas the ranges are 0.62–1.85 μmol·m^{-2}·s^{-1} (spring–summer) and 0.02–0.05 μmol·m^{-2}·s^{-1} (winter–summer) in Ku1 and 0.50–2.93 μmol·m^{-2}·s^{-1} (winter–summer) and 0.01–0.07 μmol·m^{-2}·s^{-1} (winter–fall) in Ku3.

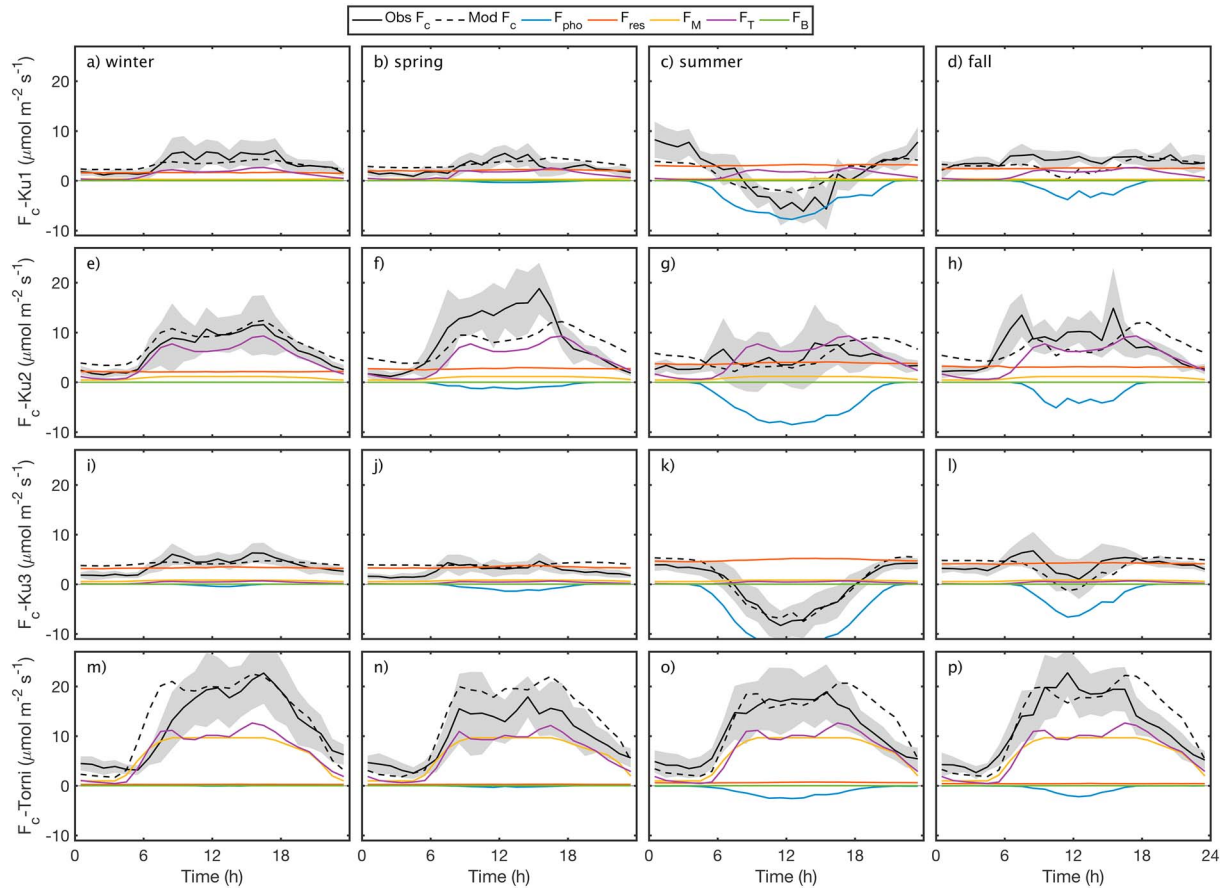

Figure 3. Median (lines) diurnal behavior of measured and modeled carbon dioxide flux (F_c, μmol·m^{-2}·s^{-1}) and its components at Kumpula (a–d) built (Ku1), (e–h) road (Ku2), (i–l) vegetation (Ku3) sectors, and (m–p) at Hotel Torni for different thermal seasons. CO_2 emissions/sink from photosynthesis (F_{pho}), respiration (F_{res}), human metabolism (F_M), traffic (F_T), and buildings (F_B). Gray areas show the quartile deviation ((*Q3*–*Q1*)/2, where *Q3* and *Q1* are the third and first quartiles) of the measured F_c.

For Ku1, the observed daytime maximum is 8.2 μmol·m^{-2}·s^{-1} in winter compared to the smaller simulation maximum 4.5 μmol·m^{-2}·s^{-1} (Figure 3a). Road traffic is the largest source of CO_2 with modeled maximum 2.7 μmol·m^{-2}·s^{-1}. The only exception is summer when soil respiration reaches 3.3 μmol·m^{-2}·s^{-1}. In summer, the maximum vegetation sink is −7.7 μmol·m^{-2}·s^{-1}. The other sources (soil and vegetation respiration, heating and human metabolism) stay below 2.6 μmol·m^{-2}·s^{-1} throughout the year. For Ku2, the observed daytime maximum 18.8 μmol·m^{-2}·s^{-1} is measured in spring with simulated value 12.2 μmol·m^{-2}·s^{-1}. In summer, the observed and modeled maxima are 7.9 and 9.0 μmol·m^{-2}·s^{-1}, but the timing of the maxima are slightly off. The effect of road traffic on the net CO_2 emission is clear with maximum 9.3 μmol·m^{-2}·s^{-1} in daytime. Despite the large vegetation sink (−8.5 μmol·m^{-2}·s^{-1}) in summer, vegetation is not able to offset the emissions in the area. Emissions from respiration, human metabolism, and building heating stay below 4.1 μmol·m^{-2}·s^{-1}. The model captures F_c well in summer in the most vegetated sector Ku3 where the lowest MAE occurs (0.06 μmol·m^{-2}·s^{-1}) when compared to other seasons. The observed and modeled daily maximum sinks are −8.3 and −7.5 μmol·m^{-2}·s^{-1}, respectively. Vegetation uptake reaches −13.5 μmol·m^{-2}·s^{-1} and soil and vegetation respiration 5.2 μmol·m^{-2}·s^{-1} in summer. In fall, the effect of vegetation is still evident in the middle of the day, but the net flux stays positive. Anthropogenic emissions are below 0.81 μmol·m^{-2}·s^{-1} throughout the year.

Within the model, the ratio of growing-season daily vegetation CO_2 uptake to evaporation, a measure of ecosystem water-use efficiency (WUE), is 2.4 g C·kg^{-1} H_2O at Ku3. This value, when scaled by the fractional cover of vegetation, falls within the range of WUE observed in northern temperate forests (Law et al., 2002). In general, the modeled biogenic components in Kumpula are similar in magnitude to values obtained in highly vegetated EC site in Minneapolis with a different approach (Menzer & McFadden, 2017).

Table 3
Model Evaluation Statistics for F_c at Ku1, Ku2, Ku3, and Torni by Season

Site	Season	*r*	RMSE	nRMSE	MAE	nMAE	Mean	*N*
Ku1	Winter	0.45	0.69	0.021	0.65	0.019	3.74	562
	Spring	0.52	0.62	0.037	0.46	0.028	2.93	342
	Summer	0.67	1.85	0.048	1.46	0.038	3.35	372
	Fall	0.10	1.31	0.038	1.69	0.049	4.67	197
Ku2	Winter	0.69	2.10	0.026	0.41	0.005	7.00	1342
	Spring	0.51	2.35	0.030	1.28	0.016	8.85	409
	Summer	0.31	3.00	0.040	0.10	0.001	4.99	905
	Fall	0.08	2.65	0.066	0.17	0.004	6.94	227
Ku3	Winter	0.36	0.50	0.009	0.35	0.006	3.79	1008
	Spring	0.17	0.91	0.020	1.11	0.024	2.66	815
	Summer	0.84	2.93	0.066	0.06	0.001	−0.11	1917
	Fall	0.48	2.63	0.070	0.46	0.012	3.80	370
Torni	Winter	0.65	5.61	0.061	0.21	0.002	11.60	1308
	Spring	0.66	5.38	0.081	1.13	0.017	10.39	759
	Summer	0.63	5.27	0.061	0.24	0.003	11.51	2160
	Fall	0.61	5.62	0.113	0.58	0.012	12.08	586

Note. Statistics are a Pearson correlation coefficient (*r*), root-mean-square error (RMSE, $\mu mol \cdot m^{-2} \cdot s^{-1}$), normalized root mean square error (nRMSE), mean absolute error (MAE, $\mu mol \cdot m^{-2} \cdot s^{-1}$), normalized mean absolute error (nMAE), observed mean F_c ($\mu mol \cdot m^{-2} \cdot s^{-1}$), and number of hours evaluated (*N*).

In the city center, the diurnal behavior is also well simulated with nRMSE between 0.06–0.11 (winter–fall) and MAE between 0.21–1.13 $\mu mol \cdot m^{-2} \cdot s^{-1}$ (winter–spring). In winter the best model performance is seen with nMAE 0.02 $\mu mol \cdot m^{-2} \cdot s^{-1}$. The observed and modeled daytime maxima 22.7 and 22.5 $\mu mol \cdot m^{-2} \cdot s^{-1}$ are measured in winter. Emission from road traffic reach 12.6 $\mu mol \cdot m^{-2} \cdot s^{-1}$ during the rush hours and together with human metabolism (daytime maximum 9.6 $\mu mol \cdot m^{-2} \cdot s^{-1}$) is the largest source for CO_2. In winter the modeled F_c starts to increase earlier in the morning than the observed F_c. The observed CO_2 flux is delayed because of weak turbulent mixing in the early morning in winter. The same effect has also been seen with particle fluxes at the same site (Kurppa et al., 2015). Vegetation sink is maximum -2.6 $\mu mol \cdot m^{-2} \cdot s^{-1}$ in summer while soil and vegetation respiration and building heating emissions remain below 0.7 $\mu mol \cdot m^{-2} \cdot s^{-1}$. SUEWS overestimates the evening emissions because of the combined effects from traffic and human metabolism particularly in summer and fall. In future, more detailed information about the movement and activity of people is needed.

Not unexpectedly, the model has difficulties predicting extreme F_c as the detailed dynamics of the anthropogenic emission sources (population density and traffic rate) are not captured. The modeled annual cumulative carbon emission (1,440 g $C \cdot m^{-2} \cdot year^{-1}$) in Kumpula is 2% higher that the observed gap-filled value (1,414 g $C \cdot m^{-2} \cdot year^{-1}$). Expectedly, these are smaller than the city center F_c (4,640 g $C \cdot m^{-2} \cdot year^{-1}$), which is 3% higher than the gap-filled observed value (4,507 g $C \cdot m^{-2} \cdot year^{-1}$). However, the EC measured CO_2 exchange values have random and systematic uncertainties. The random uncertainty, related to the stochastic nature of the turbulence, is estimated to be 10–20% in typical atmospheric conditions (Rannik et al., 2016). However, this should cancel out in annual totals leaving the systematic uncertainties as error sources. Errors in the annual totals of ecosystem CO_2 exchange above vegetated ecosystems are estimated to be 15–60% (Balldocchi, 2003). At Torni an underestimation of 12% has been reported resulting from removal of data from a relatively wide flow distortion area (Järvi et al., 2018). Thus, we can conclude that SUEWS simulates the net CO_2 surface exchange well at the two sites in Helsinki.

5.2. Spatial Variability of CO_2 Surface Exchange in Helsinki

The map of annual total F_c has distinct spatial variability (Figure 4a). The city center is clearly distinguished as a hot spot with a maximum emission of 10,474 g $C \cdot m^{-2} \cdot year^{-1}$. In the same grid, human metabolism is the largest contributor to the net emissions (9,103 g $C \cdot m^{-2} \cdot year^{-1}$), followed by road traffic (1,357 g $C \cdot m^{-2} \cdot year^{-1}$). The YKR data can overestimate the number of people in certain areas as it can assume that

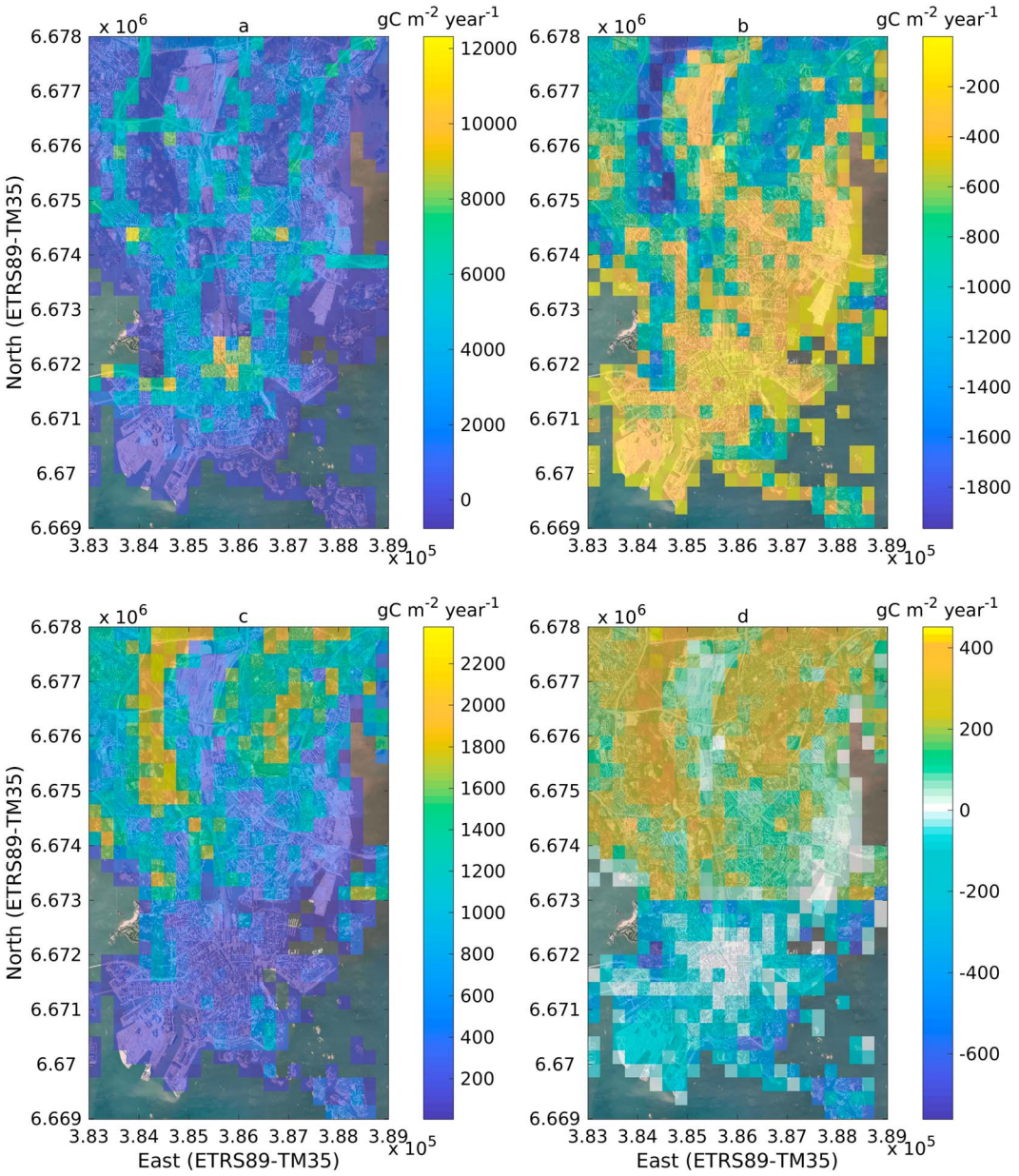

Figure 4. Annual cumulative (a) net CO_2 flux (F_c), (b) photosynthesis (F_{pho}), (c) respiration (F_{res}), and (d) biogenic net CO_2 ($F_{c,bio}$) flux for 2012. All have units g C·m^{-2}·year^{-1}, but scale differs between maps.

all employees are located in the headquarter of a company even though in reality they are situated in different offices. Other hot spots are west of the city center (11,558 g C·m^{-2}·year^{-1}), where a major access road with an annual emission of 6,192 g C·m^{-2}·year^{-1} and some company headquarters are located, and the hospital area (12,328 g C·m^{-2}·year^{-1}) where the emissions are mainly related to human metabolism (10,900 g C·m^{-2}·year^{-1}). In the hospital, three shifts per day are common causing an overestimation as not all people are present at the same time. Overall, the access roads are clearly visible because of the high traffic volumes. Although, the highly vegetated areas are visible the biogenic components are an order of magnitude smaller than the anthropogenic emissions (Figures 4b and 4c). In 252 (29 %) grids photosynthesis offsets the soil and vegetation respiration resulting in negative NEE (maximum −762 g C·m^{-2}·year^{-1}). These areas concentrate in the city center where there is less organic matter to respire. In the Helsinki central park (urban forest in the northwest corner) NEE remains mainly positive with maximum photosynthesis -1,967 g C·m^{-2}·year^{-1} but at the same time, vegetation and soil respiration is 2,363 g C·m^{-2}·year^{-1} resulting in NEE

of 396 g C·m^{-2}·year^{-1}. Only in summer is the vegetation sink able to offset the emissions from respiration with a maximum sink of −1,680 g C·m^{-2}·year^{-1} and respiration of 1,138 g C·m^{-2}·year^{-1} resulting in NEE of −541 g C·m^{-2}·year^{-1}.

The magnitude of road traffic emission hot spots in central Helsinki are similar to eastern Massachusetts (Brondfield et al., 2012) but generally less than the Boston region where emissions hot spots exceed 25 000 g C·m^{-2}·year^{-1} (Gately et al., 2017). An hourly 1 km resolution daily maxima value 55 g C·m^{-2}·day^{-1} (October 2008) in Paris (Bréon et al., 2015) are larger than the equivalent in Helsinki (33 g C·m^{-2}·day^{-1})

5.3. Total Areal Emissions

The total amount of carbon emitted to the atmosphere from the study area is 81.8 kt C·year^{-1}. The largest emission source is road traffic with a net emission of 49.6 kt C·year^{-1} followed by human metabolism 31.6 kt C·year^{-1}. Local emissions from building energy production are only 0.003 kt C·year^{-1} as heating and energy are mainly centrally produced in Helsinki. The vegetation sink is −29.0 kt C·year^{-1} and respiration is 31.8 kt C·year^{-1} resulting in NEE of 2.8 kt C·year^{-1}. There is one power plant within the study area, but as its stack height is 150 m (i.e., 7–8 times the mean building height) the emissions are mostly above the surface layer of interested here. Hence they are not included. When the boundary layer depth is high, these emissions will be mixed in to the background urban values. When the boundary layer is very low (e.g., winter stable conditions), these emissions would need to be entrained back into the boundary layer to impact the area. The intent of the tall stack is to ensure the emissions are lost to downwind areas beyond the immediate local-scale vicinity.

The contributions of different local-scale anthropogenic emission sources within the study domain are in decreasing order road traffic (61%), human metabolism (39%), and heating and energy production (∼ 0%). This is consistent with the concern that human and animal respiration is significant and underestimated in bottom-up estimates of urban CO_2 emissions (Gately et al., 2017). In central London, road traffic has been found to be the greatest source contributing 70% to the net CO_2 spatial emissions, followed by building activities (16%) and human metabolism (14%; Björkegren & Grimmond, 2018). Within the source areas of EC measurements, large contribution for human metabolism (38%) was found in Tokyo, Japan, (Moriwaki & Kanda, 2004) and small (5%) in Vancouver, Canada (Crawford & Christen, 2015), and (<2%) in Minneapolis-Saint Paul, USA (Menzer & McFadden, 2017). The total spatial carbon emission per unit area (5.7 kg C·m^{-2}·year^{-1}) is nearly the same (5.6 kg C·m^{-2}·year^{-1}) as in Boston region (Gately et al., 2017) but smaller than reported for central London (12.7–14.5 kg C·m^{-2}·year^{-1}; Ward et al., 2015; Björkegren & Grimmond, 2018).

5.4. Anthropogenic Model Uncertainties

Uncertainties in simulating human metabolic emissions originate from the estimation of population densities and the value of metabolic CO_2 release per person. Unfortunately, we do not have uncertainty estimates for the first database used in this study. As Gately et al. (2017) note, generally uncertainties for the data required to estimate urban emissions are rarely available which makes the questification of uncertainty in emissions difficult. However, we can estimate the uncertainty in the metabolic CO_2 release per person. If we use a daily mean value of 251 g C·day^{-1} (Prairie & Duarte, 2007) instead of the current values (Table 2), the areal emission from human metabolism is 29.7 kt C·year^{-1} or 6% lower than the original estimate.

Uncertainties in traffic emissions originate from the emission factors used and the traffic rates. In the simulations, a single emission factor (0.285 kg·km^{-1}) estimated for Helsinki is used as more detailed spatially variable values are not available. For Ku2, we estimate a local emission factor from annual traffic data using information on the vehicle types on each road. Combining these we estimate an emission factor of 0.298 kg·km^{-1}. Given the linear dependence of traffic emissions on E_c, the 4% difference in E_c results in a 4% difference in traffic emissions for this particular area. Using hourly traffic data (Järvi et al., 2012) for Ku2, the annual emissions are 1,625 kt C·year^{-1}or 1.5 % smaller than simulated using mean traffic rate (1,649 kt C·year^{-1}).

Building emissions are calculated using heating degree days and building energy use emission factors. The uncertainty in coefficient $a_{2,d}$ (Appendix C) gives an areal emission of 0 to 0.004 kt C·year^{-1} compared to 0.003 kt C·year^{-1}. The hard wood emission factor used for building energy use is selected as this is the main emission source in the studied area. Similar to traffic, building emissions are linearly dependent on the emission factor.

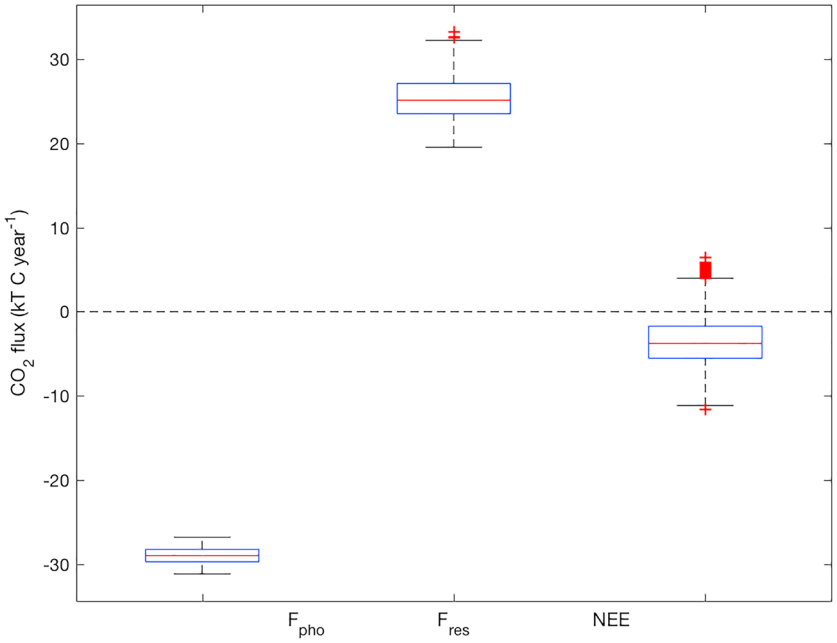

Figure 5. Boxplots of vegetation uptake (F_{pho}), vegetation and soil respiration (F_{res}), and net ecosystem exchange (NEE) made with the parameter uncertainties used to calculate F_{pho} and F_{res}. Whiskers are 5th and 95th percentiles.

5.5. Biogenic Flux Model Sensitivity

The challenge in estimating annual NEE is that it is a difference between two large values, F_{res} and F_{pho}. Thus, even small uncertainties in their estimation can result in large errors in NEE. For each grid, we estimated the parameters based on Helsinki observations. These estimates cannot capture all soil variability within a city but act as a first step in using urban parameterizations in estimating biogenic components in urban areas. To test the sensitivity of NEE to F_{res} and F_{pho}-related parameters, SUEWS is run across the spatial domain with perturbed parameters based on measurements (Table A1).

F_{res} has larger variability than F_{pho} ranging between 19.5 and 33.2 kt C·year^{-1} compared to −26.8 and −31.2 kt C·year^{-1} (Figure 5). This greater variability originates from the larger scatter in the measured data used to calculate the parameters for respiration than for photosynthesis. Using different combinations of F_{res} and F_{pho} to calculate NEE, we get a median value of 0.76 ± 1.9 kt C·year^{-1}. Thus, on an annual basis vegetation is likely a source in Helsinki, but given the uncertainties of the parameters used to calculate biogenic fluxes in the study domain, it could act as either a source or a sink.

6. Conclusions

In this study, the surface-atmosphere exchange of CO_2 is incorporated into the urban land surface model SUEWS. This complements the surface energy and water balance capability of the model allowing examination of the connections between energy, water, and CO_2 exchanges at the local scale. The model contains both anthropogenic and biogenic components. The biogenic parameters are derived from urban observations to ensure urban effects are accounted for. The model is evaluated in Helsinki using EC observations from two sites representing four different urban surface covers. The high spatial and temporal variability and magnitude of local-scale carbon emissions and sinks in central Helsinki are studied using a combination of sources for surface data. These include surface cover fractions derived from 2-m resolution airborne lidar scanning, traffic data, and separate nocturnal, and daytime population densities derived from novel mobility data. Building energy use is calculated from heating and cooling degree days-based anthropogenic heat flux model minimizing the input data needed.

SUEWS simulates the correct diurnal and seasonal behavior for the net CO_2 surface exchange over different urban land uses. In suburban areas, road traffic is a dominant source for CO_2 which is nearly countered by vegetation uptake in summer. In the city center, road traffic and human metabolism account for nearly equal shares but given the low fraction of vegetated surfaces (22%) the ability of vegetation to offset these

emissions is small. The large difference between daytime (466,000) and nighttime (179,000) populations in central Helsinki causes CO_2 emissions from human metabolism to be 39% of the net local-scale emissions in this area. If human metabolism was to be neglected, this can lead to a significant bias both in net emissions and the spatial variability of the CO_2 surface exchange. Carbon inversion studies need this component to be included as the anthropogenic CO_2 emissions are used as a boundary condition. Thus, estimation of the magnitude and spatial variability of human emissions is highly dependent on a good understanding of population mobility and distribution. Note that most of Helsinki's energy is produced in two large power plants whose emissions do not get captured in a local-scale model.

The largest carbon source in a local scale in central Helsinki is road traffic (50 kt C·year^{-1}) and human metabolism (32 kt C·year^{-1}). On an annual basis, vegetation acts as a net source for CO_2 (2.8 kt C·year^{-1}). This is partly caused by the short growing season in Helsinki allowing for less photosynthetic uptake relative to soil and vegetation respiration and partly by changes in other environmental variables. This suggests that in high-latitude cities vegetation may have limited potential to sequester CO_2 from the atmosphere. However, in order to quantify the seasonal and spatial variations in urban CO_2 emissions and to understand the detailed urban biogenic carbon cycle and its different components (respiration, storage, and photosynthesis), detailed models accounting for the highly variable soil and vegetation structure are needed.

We have demonstrated that SUEWS can be used to study high temporal (hourly) and spatial (250 m × 250 m) variability of local-scale CO_2 in urban ares. Thus, it can be used to estimate the effectiveness of different urban planning scenarios on local-scale carbon emissions at different spatial scales by answering questions such as which type of vegetation would maximize carbon storage or what would be the effect of transforming roads to bike lanes. SUEWS in a standalone mode is not intended to examine the total carbon budgets for a city including emissions from airports, nonlocal power plants, or other nonlocal sources but rather can provide a detailed local-scale emissions and their temporal and spatial variability that emission inventories or top-down emission estimates often ignore or simplify. To estimate realistic local-scale anthropogenic CO_2 emissions, the details on the emission sources and emission strengths are key to applying the model in different cities and areas. Also, as the biogenic parameters will vary with plant functional types using the Helsinki values may not produce the correct vegetation uptake and respiration behavior.

Appendix A: Parameterization of Biogenic Model Components

In empirical canopy-level photosynthesis models as used in SUEWS (equation (10)), the different responses on environmental variables can be statistically estimated from observations (Mäkelä et al., 2008). For the response functions of F_{pho} on $K_\downarrow$ ($f(K_\downarrow)$), Δq ($f(\Delta q)$), $\Delta\theta$ ($f(\Delta\theta)$), and T_{air} ($f(T_{air})$) we use those used in SUEWS to calculate of surface conductance (Ward et al., 2016)

$$f(\Delta q) = \frac{K_\downarrow/(G_2 + K_\downarrow)}{K_{\downarrow,max}/(G_2 + K_{\downarrow,max})}, \tag{A1}$$

$$f(\Delta q) = G_3 + (1 - G_3)G_4^{\Delta q}, \tag{A2}$$

$$f(T_{air}) = \frac{(T_{air} - T_L)(T_H - T_{air})^{T_C}}{(G_5 - T_L)(T_H - G_5)^{T_C}}, \tag{A3}$$

where

$$T_C = \frac{(T_H - G_5)}{(G_5 - T_L)}, \tag{A4}$$

and

$$f(\Delta\theta) = \frac{1 - \exp(G_6(\Delta\theta - \Delta\theta_{WP}))}{1 - \exp(-G_6\Delta\theta_{WP})}. \tag{A5}$$

In equations, parameters G_2–G_6 describe the responses of F_{pho} on each environmental variable, $K_{\downarrow,max}$ is the maximum observed solar radiation, $\Delta\theta_{WP}$ is the wilting point, and T_L and T_H are the lower and upper limits

Table A1
Model Parameters Used to Simulate Photosynthesis and Respiration in Helsinki Using SUEWS

Parameter	Kumpula	Torni	Reference
$\Delta\theta_{WP}$ (mm)	120	120	Ward et al. (2016)
G_2 (W·m^{-2})	566.1	566.1	Järvi et al. (2014)
G_3 (-)	0.2427	0.5596	This study
G_4 (-)	0.4362	0.9373	This study
G_5 (°C)	30	30	Ward et al. (2016)
G_6 (mm)	0.05	0.05	Ward et al. (2016)
$K_{\downarrow,max}$ (W·m^{-2})	1200	1200	Järvi et al. (2014)
T_L (°C)	−10	−10	Ward et al. (2016)
T_H (°C)	55	55	Ward et al. (2016)
$a_{evergtr}$ (-)	5.295 ± 0.391	5.295 ± 0.391	Bellucco et al. (2017)
$b_{evergtr}$ (-)	0.03 ± 0.01	0.03 ± 0.01	Bellucco et al. (2017)
$a_{decidtr}$ (-)	5.295 ± 0.391	0.519 ± 0.001	Bellucco et al. (2017)/This study
$b_{decidtr}$ (-)	0.03 ± 0.01	0.0896 ± 0.0002	Bellucco et al. (2017)/This study
a_{grass} (-)	5.295 ± 0.391	2.1 ± 0.8	Bellucco et al. (2017)/Järvi et al. (2011)
b_{grass} (-)	0.03 ± 0.01	0.06 ± 0.03	Bellucco et al. (2017)/Järvi et al. (2011)
$F_{pho,max,evergtr}$ (μmol·m^{-2}·s^{-1})	29.2138 ± 2.2536	29.2138 ± 2.2536	This study
$F_{pho,max,decidtr}$ (μmol·m^{-2}·s^{-1})	27.0891 ± 2.0897	6.739 ± 0.021	This study
$F_{pho,max,grass}$ (μmol·m^{-2}·s^{-1})	25.2526 ± 1.9480	25.2526 ± 1.9480	This study
$LAI_{evergtr,max}$ (m^2·m^{-2})	5.1	5.1	Järvi et al. (2011)
$LAI_{decidtr,\ max}$ (m^2·m^{-2})	5.5	5.5	Järvi et al. (2011)
$LAI_{grass,\ max}$ (m^2·m^{-2})	5.9	5.9	Järvi et al. (2011)

Note. See Notation for details. SUEWS = Surface Urban Energy and Water balance Scheme.

when photosynthesis and evaporation switch off (Table A1). Values for G_2, G_5, and G_6 from past studies provide reasonable responses for F_{pho} in Helsinki. However, for specific humidity, values of $f(\Delta q)$ are too low. Therefore, we fit parameters G_3 and G_4 together with the potential photosynthesis ($F_{pho,max}$) using Helsinki observations, to obtain appropriate estimates of F_{pho} in SUEWS (equation (10)).

For urban forest and park area (Ku3), the parameters are determined by fitting equation (10) against EC observations from Kumpula in 2006–2011. The environmental variables $K_\downarrow$, T_{air} and Δq are measured at the site, whereas $\Delta\theta$ modeled values are used (Järvi et al., 2017). LAI and surface fraction of each vegetation type i are only considered after the fitting has been made (see below). Following Bellucco et al. (2017), summer (June–August) weekend days from the most vegetated direction in Ku3 (200–270°) are used in the nonlinear fit. The data selection is to minimize the anthropogenic effects on net CO_2 exchange measured by the EC technique. After commonly accepted quality control procedures including removal of spikes and stationary test with limit 60% (Nordbo et al., 2012b), there are 597 sixty-minute data points for analysis. Soil and vegetation respiration estimated from equation (11) is reduced from the net flux.

As parameter values we use $a_i = 5.295 \pm 0.391$ and $b_i = 0.03 \pm 0.01$ obtained from nocturnal EC data in the same vegetated direction (Bellucco et al., 2017). The model parameter uncertainties are estimated using bootstrapping with 7/8th of the data selected randomly 100 times to be used in the nonleast squares fitting (Matlab function lsqcurvefit). This gives values $G_3 = 0.243 \pm 0.014$, $G_4 = 0.436 \pm 0.029$, and $F_{c,pho,max} = 90.884 \pm 7.011$ μmol·m^{-2}·s^{-1}. Furthermore, $F_{c,pho,max}$ is scaled with the maximum LAI and to 100% for each vegetation type, resulting in vegetation specific values (Table A1).

Using the Table A1 parameter values, SUEWS simulates F_{pho} well for the independent summer of 2012 for Ku3 with RMSE = 3.0 μmol·m^{-2}·s^{-1} and $R^2 = 0.88$ (Figure A1). Radiation and specific humidity have the largest impact on F_{pho} with $f(K_\downarrow)$ and $f(\Delta q)$ between 0–0.97 and 0.28–0.88, followed by $f(T_{air})$ (0.63–0.99) and $f(\Delta\theta)$ (0.98–0.99).

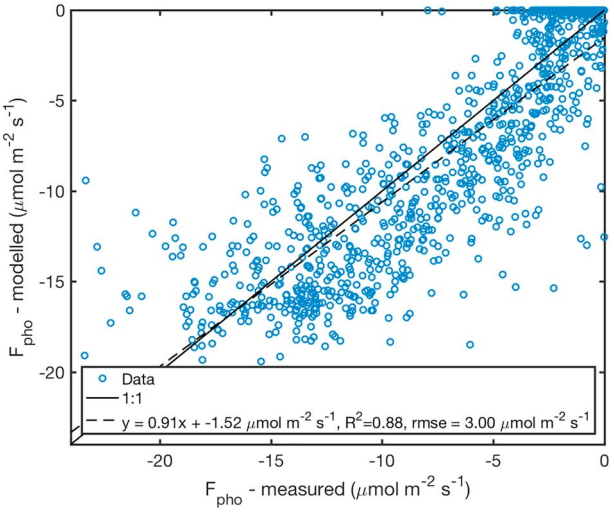

Figure A1. Correlation between the measured and modeled photosynthesis (F_{pho}) in Ku3 (180–320°) in summer 2012. Data are 60-min values ($N = 1187$).

Parameters G_3, G_4, and $F_{pho,max,decitr}$ for deciduous street trees in Helsinki are determined with the aid of leaf-level photosynthetic responses measured for the planted common lime (*Tilia x vulgaris*) during five field campaigns in 2007–2009 (Riikonen et al., 2011). In each campaign, a total of 22–25 leaf samples from six to seven trees was measured with portable gas exchange sensor (CIRAS-2, PP Systems, UK). The measured responses are scaled to stand level using the forest stand gas exchange model SPP (Mäkelä et al., 2006) for a typical summer in Helsinki (2012). From the several SPP photosynthesis and stomatal control models, the optimal stomatal control model (Hari et al., 1986) was employed. The input data for SPP (photosynthetically active radiation, air temperature, humidity, and CO_2) are from Kumpula. Soil water is not explicitly considered, that is, set to a value where soil moisture will not affect the gas exchange of vegetation. The stand level $LAI_{decidtr}$ is assumed to be 6 $m^2 \cdot m^{-2}$.

The stand level F_{pho} 30-min values used with equation (10) and the Kumpula $K_{\downarrow}$, T_{air} and Δq, and observed $\Delta\theta$ from the street where the trees were planted in 2016 (Riikonen et al., 2016) are used to get model parameters for city centre. Using bootstrapping (as above), we get $G_3 = 0.560 \pm 0.027$, $G_4 = 0.937 \pm 0.006$, and $F_{pho,max,\ decidtr} = 6.739 \pm 0.021$ $\mu mol \cdot m^{-2} \cdot s^{-1}$ ($N = 2884$). For the respiration parameters we get $a_{decitr} = 0.519 \pm 0.001$ and $b_{decitr} = 0.0896 \pm 0.0002$ for the city center. For grass surface, we use soil respiration parameters $a_{grass} = 2.1 \pm 0.8$ and $b_{grass} = 0.06 \pm 0.03$ measured by soil chambers in the vicinity of Kumpula EC tower (Järvi et al., 2012). These values do not consider the large spatial variability of the different vegetation types present in Kumpula. Rather, the values are obtained from carefully selected EC data (see above).

Appendix B: Estimating Minimum Soil Respiration

To minimize SUEWS input variables, air temperature is used to calculate soil respiration. This results in unrealistically low winter respiration values when soil temperature maybe warmer than air. CO_2 efflux observations from a boreal forest in Southern Finland using three automatic soil chambers are used to estimate realistic minimum values for winter time respiration. Two chambers are transparent, and one is covered to prevent radiation from entering the chamber. From the transparent chambers, only hours with no radiation are used. The chamber lids are closed for 3.5 min every 30 min, and CO_2 gas concentrations are measured with a diffusion probe (GMP343, Vaisala Oyj, Vantaa, Finland) and soil temperature with a K-type thermocouple. Between concentration sampling times, the chamber lids are tilted to the side by an electric motor. More details are given in Pumpanen et al. (2015). The minimum respiration value for 30-min periods during 2009–2012 when the measured soil temperature is below −2 °C (1,677 sampling times) is 0.60 ± 0.07 $\mu mol \cdot m^{-2} \cdot s^{-1}$.

Table C1
Parameter Values Used to Calculate $a_{0,(wd,we)}$ for EC Sites in Helsinki

Parameter	Ku1	Ku2	Ku3	Torni	Reference
$a_{0,\mathrm{wd}}$	0.1337	0.1672	0.0958	0.1105	This study
$a_{0,\mathrm{we}}$	0.1153	0.1433	0.0937	0.1084	This study
$fr_{\mathrm{QF,base,BEU,wd}}$	0.57	0.43	0.80	0.70	This study
$fr_{\mathrm{QF,base,BEU,we}}$	0.67	0.51	0.82	0.71	This study
p_{wd} (pop·ha^{-1})	19.8	39.2	36.2	212.7	This study
p_{we} (pop·ha^{-1})	23.2	38.7	38.6	182.1	This study
Tr_{wd} (veh·km·m^{-2}·day^{-1})	0.018	0.074	0.005	0.092	This study
Tr_{we} (veh·km·m^{-2}·day^{-1})	0.012	0.051	0.004	0.071	This study
$E_{h,d}$ (J·km^{-1}·veh^{-1})		$4.11 \cdot 10^6$			This study
E (W·h·cap^{-1})		$6.8 \cdot 10^6$			City of Helsinki
M_d (W·cap^{-1})		125			Sailor and Lu (2004)

Note. EC = eddy covariance.

Appendix C: Improved Coefficients for Building Heat Emissions

To improve the description of building heating-related heat and carbon emissions, the parameters $a_{0,d}$–$a_{2,d}$ in equation (6) are revisited in Helsinki using the EC measured sensible heat flux (Q_H) for the two sites (Kumpula and Hotel Torni). As air conditioning is uncommon in Helsinki, the CDD coefficient $a_{1,d}$ is set to zero. $a_{2,d}$ is estimated from hourly Q_H and air temperature data when the net all-wave radiation is $0 < Q^* < 10$ W·m^{-2}. The limit is set to minimize the contribution of Q^* and storage heat flux, which is directly dependent on Q^*, from the measured Q_H. To obtain a reasonable amount of data to determine $a_{2,d}$, data from 2006–2012 are used. At both sites, a value of 0.0149 ± 0.0147 W·ha·cap^{-1}·m^{-2} is obtained. This is nearly the same (0.01 W·ha·cap^{-1}·m^{-2}) as previously used in Helsinki (Karsisto et al., 2015).

For updated values of $a_{0,d}$ an inventory approach following Allen et al. (2011) and Ward et al. (2015) is used

$$a_{0,d} = \frac{Q_{V,d} + Q_{B,d} + Q_{M,d}}{p_d} = \frac{Tr_d E_{h,d}}{p_d} + \frac{E}{8784} + M_d, \tag{C1}$$

where $Q_{V,d}$, $Q_{B,d}$, and $Q_{M,d}$ are daily heat emissions from traffic, energy use, and human metabolism, p_d is daily population density, Tr_d traffic rate on weekdays and weekends, E_h emission factor for heat, E the net electricity consumption per capita in Helsinki, and M_d is mean daily human metabolism. The coefficient is calculated separately for the surface cover sectors at Kumpula and Hotel Torni within a 1-km radius circle from the EC measurements. Table C1 gives the parameter values used in equation (C1). Population densities are mean of the daytime and nighttime populations.

The same parameters are used to estimate the fraction of non-temperature related base Q_F from building energy use on weekdays and weekends ($fr_{\mathrm{QF,base,BEU},d}$)

$$fr_{\mathrm{QF,base,BEU},d} = \frac{Q_{B,d}}{Q_{V,d} + Q_{B,d} + Q_{M,d}}. \tag{C2}$$

Notation

Δq Specific humidity deficit (kg·kg^{-1})
$\Delta\theta$ Soil moisture deficit (mm)
$\Delta\theta_{\mathrm{WP}}$ Wilting point (mm)
a_i Empirical parameter for soil and vegetation respiration dependence on T_{air}
$a_{0,d}$ Parameter for Q_F at base temperature (W·ha·cap^{-1}·m^{-2})
$a_{1,d}$ Parameter describing CDD dependence of Q_F (W·ha·cap^{-1}·m^{-2}· K^{-1})
$a_{2,d}$ Parameter describing HDD dependence of Q_F(W·ha·cap^{-1}·m^{-2}·K^{-1})
alt Base elevation (m)
A Study area (ha)

b_i	Empirical parameter in the dependency of soil respiration on air temperature relation
cap	Capita within the study area
C_M	CO_2 release per capita ($\mu mol \cdot CO_2 \cdot s^{-1} \cdot cap^{-1}$)
$C_{M(min,max)}$	Minimum and maximum CO_2 release per capita ($\mu mol \cdot CO_2 \cdot s^{-1} \cdot cap^{-1}$)
CDD	Cooling degree days
CO_2	Carbon dioxide
d	Weekday (*wd*) or weekend (*we*)
D	Percetage change between the modeled and observed values
DLS	Day light saving
E	Net electricity consumption per capita ($Wh \cdot cap^{-1}$)
$E_{c,d}$	CO_2 release per vehicle per meter of travel ($kg \cdot km^{-1} \cdot veh^{-1}$)
$E_{h,d}$	Heat release per vehicle per meter of travel ($J\ km^{-1}\ veh^{-1}$)
E_{CO2}	CO_2 emission factor for fuels used for building heating ($\mu mol \cdot CO_2 \cdot J^{-1}$)
E_M	Energy release per capita ($W \cdot cap^{-1}$)
$E_{M(min,max)}$	Minimum and maximum value for human heat emission ($W\ cap^{-1}$)
EC	Eddy covariance
f_i	Surface fraction of *i*th surface
$f(K_\downarrow)$	Function for the dependence of stomata opening on $K_\downarrow$
$f(\Delta\theta)$	Function for the dependence of stomata opening on $\Delta\theta$
$f(\Delta q)$	Function for the dependence of stomata opening on Δq
$f(T_{air})$	Function for the dependence of stomata opening on T_{air}
F_B	CO_2 emissions from building energy use ($\mu mol \cdot m^{-2} \cdot s^{-1}$)
F_c	Net CO_2 flux ($\mu mol \cdot m^{-2} \cdot s^{-1}$)
$F_{c,ant}$	Anthropogenic CO_2 flux ($\mu mol \cdot m^{-2} \cdot s^{-1}$)
$F_{c,bio}$	Biogenic CO_2 flux ($\mu mol \cdot m^{-2} \cdot s^{-1}$)
$F_{c,mod}$	Modeled net CO_2 flux ($\mu mol \cdot m^{-2} \cdot s^{-1}$)
$F_{c,obs}$	Observed net CO_2 flux ($\mu mol \cdot m^{-2} \cdot s^{-1}$)
$F_{pho,max,i}$	Potential photosynthesis ($\mu mol \cdot m^{-2} \cdot s^{-1}$)
F_M	CO_2 emission from human metabolism ($\mu mol \cdot m^{-2} \cdot s^{-1}$)
$F_{M,h,d}$	Hourly CO_2 emission from human metabolism on workday/weekend ($\mu mol \cdot m^{-2} \cdot s^{-1}$)
F_P	CO_2 emission from stationary single-point sources ($\mu mol \cdot m^{-2} \cdot s^{-1}$)
F_{pho}	Photosythesis ($\mu mol \cdot m^{-2} \cdot s^{-1}$)
$Fres$	Soil and vegetation respiration ($\mu mol \cdot m^{-2} \cdot s^{-1}$)
F_V	CO_2 emissions from road traffic ($\mu mol \cdot m^{-2} \cdot s^{-1}$)
$F_{V,h,d}$	Hourly CO_2 emissions from road traffic on workdays/weekends ($\mu mol \cdot m^{-2} \cdot s^{-1}$)
fr_{build}	Plan area fraction of buildings within the study area
$fr_{decidtr}$	Plan area fraction of deciduous trees/shrubs within the study area
$fr_{evergtr}$	Plan area fraction of evergreen trees/shrubs within the study area
fr_{grass}	Plan area fraction of grass within the study area
fr_{paved}	Plan area fraction of paved surfaces within the study area
fr_{water}	Plan area fraction of water surfaces within the study area
fr_{heat}	Fraction of fossil fuels used for building heating relative to district heating
$fr_{nonheat}$	Fraction of fossil fuels used for energy consumption relative to district heating
$fr_{QF,base,BEU,d}$	Fraction of building energy use from $Q_{F,base}$
G_{2-6}	Parameters describing the response of photosynthesis on different environmental factors
h	Hour
$H_{A,d}$	Diurnal activity profile on different days
$H_{A,h,d}$	Activity per hour calculated from the activity and population profiles
$H_{P,d}$	Diurnal profile for population density on different days
$H_{T,d}$	Diurnal traffic profile on different days
HDD	Heating degree days
i	Vegetation type
$K_\downarrow$	Shortwave radiation ($W \cdot m^{-2}$)
$K_{\downarrow,max}$	Maximum shortwave radiation ($W \cdot m^{-2}$)
Ku1	Kumpula northern land use sector

Ku2	Kumpula eastern land use sector
Ku3	Kumpula southwestern land use sector
LAI_i	Leaf area index of *i*th vegetation type (m^2 m^{-2})
LCZ	Local Climate Zone (Stewart & Oke, 2012)
M_d	Mean daily human metabolism ($W \cdot cap^{-1}$)
MAE	Mean absolute error ($\mu mol \cdot m^{-2} \cdot s^{-1}$)
nMAE	Normalized mean absolute error (-)
nRMSE	Normalized root mean square error (-)
N	Number of data points
NEE	Net ecosystem exchange
p_d	Mean population density within study area on weekdays and weekends ($cap \cdot ha^{-1}$)
$p_{h,d}$	Population density within the study area per hour per day ($cap \cdot ha^{-1}$)
$Q*$	Net all-wave radiation ($W \cdot m^{-2}$)
$Q_{B,d}$	Heat emissions from buildings on workdays/weekends ($W \cdot m^{-2}$)
$Q_{B,h,d}$	Hourly heat emissions from buildings o workdays/weekends ($W \cdot m^{-2}$)
Q_F	Anthropogenic heat flux ($W \cdot m^{-2}$)
$Q_{F,\mathrm{base}}$	Non-temperature related anthropogenic heat flux (W/m^{-2})
$Q_{F,\mathrm{cool}}$	Anthropogenic heat flux related to CDD (W/m^{-2})
$Q_{F,\mathrm{heat}}$	Anthropogenic heat flux related to HDD (W/m^{-2})
Q_H	Sensible heat flux (W/m^2)
$Q_{M,d}$	Heat emissions from human metabolism (W/m^{-2})
$Q_{M,h,d}$	Hourly heat emissions from human metabolism on workdays/weekends ($W \cdot m^{-2}$)
$Q_{V,d}$	Heat emissions from road traffic (W/m^{-2})
$Q_{V,h,d}$	Hourly heat emissions from road traffic on workdays/weekends ($W \cdot m^{-2}$)
r	Pearson correlation coefficient
R^2	Squared Pearson correlation coefficient
RMSE	Root mean square error ($\mu mol \cdot m^{-2} \cdot s^{-1}$)
SUEWS	the Surface Urban Energy and Water balance Scheme
T_{air}	Air temperature (°C)
T_C	Air temperature fraction needed to calculate the response of stomata opening on air temperature
T_H	Upper limit when photosynthesis and evaporation switch off (°C)
T_L	Lower limit when photosynthesis and evaporation switch off (°C)
Tr_d	Daily traffic rate on weekdays/weekends ($veh \cdot km \cdot m^{-2} \cdot day^{-1}$)
z	EC measurement height (m)
z_{build}	Mean height of buildings within the study area (m)
z_{tree}	Mean height of trees within the study area (m)
wd	Weekdays
we	Weekends
WUE	Water Use Efficiency ($g\ C\ kg^{-1}$)

Acknowledgments
The work was supported by the Academy of Finland project ICOS-Finland, the Center of Excellence programme (Grant 307331), and EPSRC LoHCool (EP/N009797/1). We also thank Sokos Hotel Torni for allowing us to use their building for our EC measurements. Data can be downloaded online http://doi.org/10.5281/zenodo.2572472.

References

Alexander, P. J., Bechtel, B., Chow, W. T. L., Fealy, R., & Mills, G. (2016). Linking urban climate classification with an urban energy and water budget model: Multi-site and multi-seasonal evaluation. *Urban Climate*, *17*, 196–215. https://doi.org/10.1016/j.uclim.2016.08.003

Allen, L., Lindberg, F., & Grimmond, C. S. B. (2011). Global to city scale urban anthropogenic heat flux: Model and variability. *International Journal of Climatology*, *31*, 1990–2005. https://doi.org/10.1002/joc.2210

Ao, X., Grimmond, C. S. B., Ward, H. C., Gabey, A. M., Tan, J., Yang, X.-Q., et al. (2018). Evaluation of the Surface Urban Energy and Water balance Scheme (SUEWS) at a dense urban site in Shanghai: Sensitivity to anthropogenic heat and irrigation. *Journal of Hydrometeorology*, *19*, 1983–2005. https://doi.org/10.1175/JHM-D-18-0057.1

Balldocchi, D. D. (2003). Assessing the eddy covariance technique for evaluating carbon dioxide exchange rates of ecosystems: Past, present and future. *Global Change Biology 9*, 479–492. https://doi.org/10.1046/j.1365-2486.2003.00629.x

Bellucco, V., Marras, S., Grimmond, C. S. B., Järvi, L., Sirca, C., & Spano, D. (2017). Modelling the biogenic CO_2 exchange in urban and non-urban ecosystems through the assessment of light-response curve parameters. *Agricultural and Forest Meteorology*, *236*, 113–122. https://doi.org/10.1016/j.agrformet.2016.12.011

Björkegren, A., & Grimmond, C. S. B. (2018). Net carbon dioxide emissions from central London. *Urban Climate*, *23*, 113–158. https://doi.org/10.1016/j.uclim.2016.10.002

Bréon, F. M., Broquet, G., Puygrenier, V., Chevallier, F., Xueref-Remy, I., Ramonet, M., et al. (2015). An attempt at estimating Paris area CO_2 emissions from atmospheric concentration measurements. *Atmospheric Chemistry and Physics*, *15*, 1707–1724. https://doi.org/10.5194/acp-15-1707-2015

Brondfield, M. N., Hutyra, L. R., Gately, C. K., Raciti, S. M., & Peterson, S. A. (2012). Modeling and validation of on-road CO_2 emissions inventories at the urban regional scale. *Environmental Pollution*, *170*, 113–123. https://doi.org/10.1016/j.envpol.2012.06.003

Crawford, B., & Christen, A. (2015). Spatial source attribution of measured urban eddy covariance CO_2 fluxes. *Theoretical and Applied Climatology*, *119*, 733–755. https://doi.org/10.1007/s00704-014-1124-0

Crawford, B., Grimmond, C. S. B., & Christen, A. (2011). Five years of carbon dioxide flux measurements in a highly vegetated suburban area. *Atmospheric Environment*, *45*(4), 896–905. https://doi.org/10.1016/j.atmosenv.2010.11.017

Escobedo, F., Varela, S., Zhao, M., Wagner, J., & Zipperer, W. (2010). Analyzing the efficacy of subtropical urban forests in offsetting carbon emissions from cities. *Environmental Science & Policy*, *13*, 362–372. https://doi.org/10.1016/j.envsci.2010.03.009

Gately, C. K., Hutyra, L. R., Peterson, S., & Wing, I. (2017). Urban emissions hotspots: Quantifying vehicle congestion and air pollution using mobile phone GPS data. *Environmental Pollution*, *229*, 496–504. https://doi.org/10.1016/j.envpol.2017.05.091

Grimmond, C. S. B. (1992). The suburban energy balance: Methodological considerations and results for a mid-latitude west coast city under winter and spring conditions. *International Journal of Climatology*, *12*, 481–497.

Grimmond, C. S. B., & Oke, T. R. (1991). An evaporation-interception model for urban areas. *Water Resources Research*, *27*, 1739–1755.

Gurney, K. R., Liang, J., Patarasuk, R., O'Keeffe, D., Huang, J., Hutchins, M., et al. (2017). Reconciling the differences between a bottom-up and inverse-estimated $FFCO_2$ emissions estimate in a large US urban area. *Elementa: Science of the Anthropocene*, *5*(44). https://doi.org/10.1525/elementa.137

Gurney, K. R., Razlivanov, I., Song, Y., Zhou, Y., Benes, B., & Abdul-Massih, M. (2012). Quantification of fossil fuel CO_2 emissions on the building/street scale for a large U.S. City. *Environmental Science & Technology Letters*, *42*, 12,194–12,202.

HSY (2011). SeutuCD'11 database. Helsinki Region Environmental Services Authority.

Hardiman, B. S., Wang, J. A., Hutyra, L. R., Gately, C. K., Getson, J. M., & Friedl, M. A. (2017). Accounting for urban biogenic fluxes in regional carbon budgets. *Science of the Total Environment*, *592*, 366–372. https://doi.org/10.1016/j.scitotenv.2017.03.028

Hari, P., Mäkelä, A., Korpilahti, E., & Holmberg, M. (1986). Optimal control of gas exchange. *Tree Physiology*, *2*, 169–175.

Hutyra, L. R., Duren, R., Gurney, K. R., Grimm, N., Kort, E. A., Larson, E., & Shrestha, G. (2014). Urbanization and the carbon cycle: Current capabilities and research outlook from the natural sciences perspective. *Earth's Future*, *2*, 473–495. https://doi.org/10.1016/j.scitotenv.2017.03.028

Järvi, L., Grimmond, C., & Christen, A. (2011). The surface urban energy and water balance scheme (SUEWS): Evaluation in Los Angeles and Vancouver. *Journal of Hydrology*, *411*(3-4), 219–237. https://doi.org/10.1016/j.jhydrol.2011.10.001

Järvi, L., Grimmond, C. S. B., McFadden, J. P., Christen, A., Strachan, I. B., Taka, M., et al. (2017). Warming effects on the urban hydrology in cold climate regions. *Scientific Reports*, *7*, 5833. https://doi.org/10.1038/s41598-017-05733-y

Järvi, L., Grimmond, C., Taka, M., Nordbo, A., Setälä, H., & Strachan, I. (2014). Developments of the surface urban energy and water balance scheme (SUEWS) for cold climate cities. *Geoscientific Model Development*, *7*, 1691–1711. https://doi.org/10.5194/gmd-7-1691-2014

Järvi, L., Nordbo, A., Junninen, H., Riikonen, A., Moilanen, J., Nikinmaa, E., & Vesala, T. (2012). Seasonal and annual variation of carbon dioxide surface fluxes in Helsinki, Finland, in 2006–2010. *Atmospheric Chemistry and Physics*, *12*, 8475–8489. https://doi.org/10.5194/acp-12-8475-2012

Järvi, L., Rannik, Ü., Kokkonen, T. V., Kurppa, M., Karppinen, A., Kouznetsov, R. D., et al. (2018). Uncertainty of eddy covariance flux measurements over an urban area based on two towers. *Atmospheric Measurement Techniques*, *11*, 5421–5438. https://doi.org/10.5194/amt-11-5421-2018

Karsisto, P., Fortelius, C., Demuzere, M., Grimmond, C. S. B., Oleson, K., Kouznetsov, R., et al. (2015). Seasonal surface urban energy balance and wintertime stability simulated using three land-surface models in the high-latitude city Helsinki. *Quarterly Journal of the Royal Meteorological Society*, *142*(694), 401–417. https://doi.org/10.1002/qj.2659

Kokkonen, T. V., Grimmond, C. S. B., Murto, S., Liu, H., Sundström, A.-M., & Järvi, L. (2019). Simulation of the radiative effect of haze on urban hydrological cycle using reanalysis data in Beijing. *Atmospheric Chemistry and Physics*, *19*, 7001–7017. https://doi.org/10.5194/acp-19-7001--2019

Kokkonen, T. V., Grimmond, C. S. B., Räty, O., Ward, H. C., Christen, A., Oke, T. R., et al. (2018). Sensitivity of Surface Urban Energy and Water Balance Scheme (SUEWS) to downscaling of reanalysis forcing data. *Urban Climate*, *23*, 36–52. https://doi.org/10.1016/j.uclim.2017.05.001

Korhonen, K. T., Ihalainen, A., Packalen, T., Salminen, O., Hirvelä, H., & Härkönen, K. (2015). Uudenmaan metsävarat ja hakkuumahdollisuudet (in Finnish) (*Luonnonvarakeskus (LUKE) reports*). Helsinki, Finland: Luonnonvarakeskus.

Kurppa, M., Nordbo, A., Haapanala, S., & Järvi, L. (2015). Effect of seasonal variability and land use on particle number and CO_2 exchange in Helsinki, Finland. *Urban Climate*, *13*, 94–109. https://doi.org/10.1016/j.uclim.2015.07.006

Lasslop, G., Reichstein, M., Papale, D., Richardson, A. D., Arneth, A., Barr, A., et al. (2010). Separation of net ecosystem exchange into assimilation and respiration using a light-response curve approach: Critical issues and global evaluation. *Global Change Biology*, *161*(1), 187–208. https://doi.org/10.1111/j.1365-2486.2009.02041.x

Law, B. E., Falge, E., Gu, L., Baldocchi, D. D., Bakwin, P., Berbigier, P., et al. (2002). Environmental controls over carbon dioxide and water vapor exchange of terrestrial vegetation. *Agricultural and Forest Meteorology*, *113*(1-4), 97–120. https://doi.org/10.1016/S0168-1923(02)00104-1

Lee, J. K., Christen, A., Ketler, R., & Nesic, Z. (2017). A mobile sensor network to map carbon dioxide emissions in urban environments. *Atmospheric Measurement Techniques*, *10*, 645–665. https://doi.org/10.5194/amt-10-645-2017

Loridan, T., Grimmond, C. S. B., Offerle, B. D., Young, D. T., Smith, T., Järvi, L., & Lindberg, F. (2010). Local-scale urban meteorological parameterization scheme (LUMPS): Longwave radiation parameterization and seasonality related developments. *Journal of Applied Meteorology and Climatology*, *50*, 185–202. https://doi.org/10.1175/2010JAMC2474.1

Mäkelä, A., Kolari, P., Karimäki, J., Nikinmaa, E., Perämäki, M., & Hari, P. (2006). Modelling five years of weather-driven variation of GPP in aboreal forest. *Agricultural and Forest Meteorology*, *139*, 382–398. https://doi.org/10.1016/j.agrformet.2006.08.017

Mäkelä, A., Pulkkinen, M., Kolari, P., Lagergren, F., Berbigier, P., Lindroth, A., et al. (2008). Developing an empirical model of stand GPP with the LUE approach: Analysis of eddy covariance data at five contrasting conifer sites in Europe. *Global Change Biology*, *14*, 92–108. https://doi.org/10.1111/j.1365-2486.2007.01463.x

Marcotullio, P. J., Sarzynski, A., Albrecht, J., Schulz, N., & Garcia, J. (2013). The geography of global urban greenhouse gas emissions: An exploratory analysis. *Climatic Change*, *121*(4), 621–634. https://doi.org/10.1007/s10584-013-0977-z

Menzer, O., & McFadden, J. P. (2017). Statistical partitioning of a three-year time series of direct urban net CO2 flux measurements into biogenic and anthropogenic components. *Atmospheric Environment*, *170*, 319–333. https://doi.org/10.1016/j.atmosenv.2017.09.049

Menzer, O., Meiring, W., Kyriakidis, P. C., & McFadden, J. P. (2015). Annual sums of carbon dioxide exchange over a heterogeneous urban landscape through machine learning based gap-filling. *Atmospheric Environment*, *101*, 312–327. https://doi.org/10.1016/j.atmosenv.2014.11.006

Moriwaki, R., & Kanda, M. (2004). Seasonal and diurnal fluxes of radiation, heat, water vapour, and carbon dioxide over a suburban area. *Journal of Applied Meteorology and Climatology*, *43*, 1700–1710.

Niemelä, J., Saarela, S.-R., Soderman, T., Kopperoinen, L., Yli-Pelkonen, V., Vare, S., & Kotze, D. J. (2010). Using the ecosystem services approach for better planning and conservation of urban green spaces: A Finland case study. *Biodiversity and Conservation*, *19*, 3225–3243.

Nordbo, A., Järvi, L., Haapanala, S., Moilanen, J., & Vesala, T. (2013). Intra-city variation in urban morphology and turbulence structure in Helsinki, Finland. *Boundary-Layer Meteorology*, *143*(146), 469–496. https://doi.org/10.1007/s10546-012-9773-y

Nordbo, A., Järvi, L., Haapanala, S., Wood, C. R., & Vesala, T. (2012a). Fraction of natural area as main predictor of net CO_2 emissions from cities. *Geophysical Research Letters*, *39*, L20802. https://doi.org/10.1029/2012GL053087

Nordbo, A., Järvi, L., & Vesala, T. (2012b). Revised eddy covariance flux calculation methodologies: Effect on urban energy balance. *Tellus B*, *64*, 10184. https://doi.org/10.3402/tellusb.v64i0.18184

Nordbo, A., Karsisto, P., Matikainen, L., Wood, C. R., & Järvi, L. (2015). Urban surface cover determined with airborne lidar at 2 m resolution—Implications for surface energy balance modelling. *Urban Climate*, *13*, 52–72. https://doi.org/10.1016/j.uclim.2015.05.004

Offerle, B., Grimmond, C. S. B., & Oke, T. R. (2003). Parameterization of net all-wave radiation for urban areas. *Journal of Applied Meteorology and Climatology*, *42*, 1157–1173. https://doi.org/10.1175/1520-0450

Prairie, Y. T., & Duarte, C. M. (2007). Direct and indirect metabolic CO_2 release by humanity. *Biogeosciences*, *4*, 215–217.

Pumpanen, J., Kulmala, L., Linden, A., Kolari, P., Nikinmaa, E., & Hari, P. (2015). Seasonal dynamics of autotrophic respiration in boreal forest soil estimated by continuous chamber measurements. *Boreal Environment Research*, *20*, 637–650.

Rannik, Ü., Peltola, O., & Mammarella, I. (2016). Random uncertainties of flux measurements by the eddy covariance technique. *Atmospheric Measurement Techniques*, *9*, 5163–5181.

Reckien, D., Flacke, J., Dawson, R. J., Heidrich, O., Olazabal, M., Foley, A., et al. (2014). Climate change response in Europe: What's the reality? Analysis of adaptation and mitigation plans from 200 urban areas in 11 countries. *Climatic Change*, *122*(1-2), 331–340.

Riikonen, A., Linden, L., Pulkkinen, M., & Nikinmaa, E. (2011). Post-transplant crown allometry and shoot growth of two species of street trees. *Urban Forestry & Urban Greening*, *10*(2), 87–94. https://doi.org/10.1016/j.ufug.2010.09.001

Riikonen, A., Nikinmaa, E., & Järvi, L. (2016). Environmental and crown related factors affecting street tree transpiration in Helsinki, Finland. *Urban Ecosystems*, *19*, 1693–1715. https://doi.org/10.1007/s11252-016-0561-1

Rosenzweig, C., Solecki, W., Hammer, S. A., & Mehrotra, S. (2010). Cities lead the way in climate-change action. *Nature*, *467*(7318), 909–911. https://doi.org/10.1038/467909a

Ruimy, A., Jarvis, P., Baldocchi, D., & Saugier, B. (1995). CO_2 fluxes over plant canopies and solar radiation: A review. *Advances in Ecological Research*, *26*, 1–68. https://doi.org/10.1016/S0065-2504(08)60063-X

Russo, A., Escobedo, F. J., Timilsina, N., & Zerbea, S. (2015). Transportation carbon dioxide emission offsets by public urban trees: A case study in Bolzano, Italy. *Urban Forestry & Urban Greening*, *14*(2), 398–403.

Sailor, D. J., Georgescu, M., Milne, J. M., & Hart, M. A. (2015). Development of a national anthropogenic heating database with an extrapolation for international cities. *Atmospheric Environment*, *118*, 7–18.

Sailor, D. J., & Lu, L. (2004). A top–down methodology for developing diurnal and seasonal anthropogenic heating profiles for urban areas. *Atmospheric Environment*, *38*, 2737–2748. https://doi.org/10.1016/j.atmosenv.2004.01.034

Sailor, D. J., & Vasireddy, C. (2006). Correcting aggregate energy consumption data account for variability in local weather. *Environmental Modelling & Software*, *21*, 733–738. https://doi.org/10.1016/j.envsoft.2005.08.001

Sargent, M., Barrera, Y., Nehrkorn, T., Hutyra, L. R., Gately, C. K., Jones, T., et al. (2018). Anthropogenic and biogenic CO_2 fluxes in the boston urban region. *Pnas*, *115*(29), 7491–7496. https://doi.org/10.1073/pnas.1803715115

Satterthwaite, D. (2008). Cities' contribution to global warming: Notes on the allocation of greenhouse gas emissions. *Environment & Urbanization*, *20*(2), 539–549. https://doi.org/10.1177/0956247808096127

Stewart, I. D., & Oke, T. R. (2012). Local climate zones for urban temperature studies. *Bulletin of the American Meteorological Society*, *93*, 1879–1900. https://doi.org/10.1175/bams-d-11-00019.1

Sun, T., & Grimmond, S. (2019). A Python-enhanced urban land surface model SuPy (SUEWS in Python, V2019.2): Development, deplyment and demonstration. *Geoscientific Model Development*, *12*, 2781–2795. http://doi.org/10.5194/gmd-2019-39

Tang, Y., Chen, A., & Zhao, S. (2016). Carbon storage and sequestration of urban street trees in Beijing, China. *Frontiers in Ecology and Evolution*, *12*, 53. https://doi.org/10.3389/fevo.2016.00053

Tilastokeskus (2018). Polttoaineluokitus 2018 (in Finnish) (*Tech. rep*).

Vaccari, F. P., Gioli, B., Toscano, P., & Perrone, C. (2013). Carbon dioxide balance assessment of the city of Florence (Italy), and implications for urban planning. *Landscape and Urban Planning*, *120*, 138–146. https://doi.org/10.1016/j.landurbplan.2013.08.004

Ward, H. C., Evans, J. G., & Grimmond, C. S. B. (2013). Multi-season eddy covariance observations of energy, water and carbon fluxes over a suburban area in Swindon, UK. *Atmospheric Chemistry and Physics*, *13*, 4645–4666. https://doi.org/10.5194/acp-13-4645-2013

Ward, H. C., Kotthaus, S., Grimmond, C. S. B., Björkegren, A., Wilkinson, M., Morrison, W. T. J., et al. (2015). Effects of urban density on carbon dioxide exchanges: Observations of dense urban, suburban and wood-land areas of Southern England. *Environmental Pollution*, *198*, 186–200. https://doi.org/10.1016/j.envpol.2014.12.031

Ward, H. C., Kotthaus, S., Järvi, L., & Grimmond, C. S. B. (2016). Surface urban energy and water balance scheme (SUEWS): Development and evaluation at two UK sites. *Urban Climate*, *18*, 1–32. https://doi.org/10.1016/j.uclim.2016.05.001